PHOTOCHEMICAL ETCHING
OF n-InP

By

THEODORE DOUGLAS LOWES, B.A.Sc., M.A.Sc.

A Thesis
Submitted to the School of Graduate Studies
in Partial Fulfilment of the Requirements
for the Degree
Doctor of Philosophy

McMaster University

(c) Copyright by Theodore Douglas Lowes, October 1991

DOCTOR OF PHILOSOPHY (1991)
(Materials Science and Engineering)

McMASTER UNIVERSITY
Hamilton, Ontario

TITLE: Photochemical Etching of n-InP

AUTHOR: Theodore Douglas Lowes, B.A.Sc.(Univ. of Windsor)
M.A.Sc.(Univ. of Windsor)

SUPERVISOR: Professor D.T. Cassidy, Professor A.H. Kitai

NUMBER OF PAGES: xi, 117

Abstract

The photochemical etching behaviour of n-InP was examined by producing holes or vias through the samples. The rate of material removal and quality of the resulting vias were studied as a function of: electrolyte pH, temperature, and type of metal ion impurity, illumination level, frequency, and duty cycle, sample surface quality, area, and roughness, and a second light source. The project was undertaken to prepare thin samples for the transmission electron microscope (TEM). The quality of sample produced for the TEM was acceptable, as determined by comparing the thin sections to thin sections produced by other traditional sample preparation techniques. This new method of sample preparation has the important advantages of being able to thin at a precisely predetermined region and that the resulting thin regions are surrounded by a thick built-in stabilizing structure which improves handleability.

Acknowledgements

First of all I would like to thank my advisor Dr. D.T. Cassidy for his time, advice, innovative ideas, and his ability to help and guide me through the many difficulties encountered in this project.

I would also like to express my thanks to my parents, Gerry and Gloria, for all their support throughout my academic career. Thanks also to my brothers and sisters who were always there for me, especially my brother Tom. Tom has given a whole new meaning to the concept of learning, and to life and its priorities.

Most of all I would like to thank my wife , Heather, for all her years of support and personal sacrifice allowing me to complete this thesis and pursue the things most important to me. Finally, I would like to thank Andrew for coming into our lives at a most difficult time bringing much joy and happiness. I hope that you have the opportunities to realize your dreams as I have. This thesis is dedicated to Heather and Andrew.

Table of Contents

page

Chapter 1. Introduction 1
1.1 Introduction 1
1.2 Photochemical Etching of Semiconductors . . . 4
1.3 Scope and Contents of this Thesis 6

Chapter 2. Experimental Method and Apparatus 10
2.1 Introduction 10
2.2 Sample Preparation 11
2.2.1 Surface Preparation for Photochemical Etching 12
2.2.2 Sample Preparation by Ion Milling . . . 14
2.2.3 Sample Preparation by Chemical Thinning 16
2.3 Method and Apparatus for the Production of Vias 17
2.4 Summary 24

Chapter 3. Photoetch Rate as a Function of Temperature and Illumination 25
3.1 Introduction 25
3.2 Determination of Photoetching Control 27
3.3 Illumination Effects on Photoetch Rate 35
3.4 Summary 44

Chapter 4. The Influence of Metal Ion Impurities on Photoetch Rate 46
4.1 Introduction 46
4.2 Reaction Sequence for Enhanced Photoetching . 47
4.3 Metal Ion Impurity Enhanced Photoetch Rate . . 50
4.4 Summary 57

Chapter 5. Photoetch Rate as a Function of Surface Quality and Preparation 60
5.1 Introduction 60
5.2 Photoetch Rate and Surface Preparation 61
5.3 Photoetch Rate and Surface Quality 63
5.4 Photoetch Rate and Surface Roughness 67
5.5 Summary 76

Chapter 6. On the Question of Local or Global Saturation 78
6.1 Introduction 78

6.2 Experimental 79
6.3 Evidence for Local Saturation of Photoetch Rate 81
6.4 Summary 85

Chapter 7. Photoetching for Transmission Electron Microscopy 86
7.1 Introduction 86
7.2 Sample Evaluation 86
7.3 Thickness of Photochemical Oxide 95
7.4 Application to Substrates Containing Epitaxial Layers 100
7.5 Summary 102

Chapter 8. Summary and Recommendations for Further Research 104
8.1 Introduction 104
8.2 Recommendations for Further Research 104
8.3 Summary 111

List of Figures

		page
Fig. 1.1	Schematic of a semiconductor diode laser. a) Physical dimensions of the laser and orientation of the light producing active region. b) Typical structure and dimensions of the epitaxial layers that make up a diode laser.	2
Fig. 2.1	Schematic of the experimental apparatus for via production.	18
Fig. 2.2	Rise time of the acousto optic modulator (AOM).	21
Fig. 2.3	Typical data showing detector signal versus illumination time for an etched via.	22
Fig. 3.1	Cleaved cross section of an etched via showing the self propagating waveguide.	26
Fig. 3.2	Photoetch depth versus time at 20°C, 200 Hz, and 50% duty cycle.	28
Fig. 3.3	Photoetch rate versus inverse temperature at constant irradiance, 200 Hz, and 50% duty cycle.	33
Fig. 3.4	Top view of two vias etched at a)20°C and b)50°C.	34
Fig. 3.5	Photoetch rate versus irradiance at 200 Hz, and 50% duty cycle. Solid lines represent predicted behaviour using model superimposed on experimental data where α=84, and k=255, 140, and 55 for 45°C, 35°C, and 20°C respectively. The symbols α and k are discussed in the text.	37

Fig. 3.6 Top view of an etched via highlighting features produced by defects. Note the resistance to etching at polishing scratches presumably due to carrier recombination, and small satellite vias around the perimeter believed to be caused by microscopic waveguiding. 38

Fig. 3.7 Photoetch rate versus duty cycle at 35°C. Data is for 200 Hz and 15 Hz. Solid lines represent behaviour for 15, 100, and 3200 Hz where α=84, k=140, and I=15. The symbols α, k, and I are discussed in the text. 41

Fig. 4.1 Auger electron spectra from the dark regions of photoetched GaAs confirming the presence of copper. 53

Fig. 4.2 Copper deposit on p-InP. a) Secondary electron micrograph of region directly under the incident Ar^+ laser beam. b) Confirmation of copper deposition by EDAX. 55

Fig. 4.3 Mechanical stylus profile of p-InP illuminated by Ar^+ laser beam shown in Fig. 4.2. 56

Fig. 4.4 Measured intensity profile of incident Ar^+ laser beam. 58

Fig. 5.1 Photoetch rate versus polishing powder size at 20°C, 200 Hz, and 50% duty cycle. Polishing with Br:MeOH is considered to be polishing with a powder size of 0.0 μm. 62

Fig. 5.2 Cross sectional bright field transmission electron micrographs of samples with surfaces prepared using a) Br:MeOH and b) 14.5 μm alumina powder. 65

Fig. 5.3 Dislocation depth from the free surface as a function of polishing powder size for three regimes of dislocation density i) heavy ii) moderate and iii) low dislocation density. 66

Fig. 5.4 Peak photoluminescence (PL) intensity versus polishing powder size at 14 Kelvin using 488 nm light at 2.4 mW. The peak PL signal from the Br:MeOH sample was 132 a.u. as indicated by the arrow. 68

Fig. 5.5 Top view of two vias etched under identical conditions for surfaces prepared with a) Br:MeOH and b) 14.5 μm alumina powder. . . 69

Fig. 5.6 SEM secondary electron images showing surface roughness with polishing powder size. All samples were etched with HF:HBr 5:1 by volume for 30 s at room temperature. a) Br:MeOH b) 0.05 c) 0.3 d) 1.0 e) 5.0 and f) 14.5 μm alumina powder. 71

Fig. 5.7 An example of a mechanical stylus profile illustrating how the effective surface area factor (F) was calculated. 72

Fig. 7.1 TEM micrographs of single crystal InP prepared by reactive ion milling. a) Bright field micrograph showing dark regions corresponding to indium metal islands. b) Selected area electron diffraction pattern showing polycrystalline indium metal superimposed on the single crystal InP. 89

Fig. 7.2 TEM bright field micrograph of single crystal InP prepared by ion milling at liquid nitrogen temperature. Note the absence of In islands and evidence of radiation damage. 91

Fig. 7.3 TEM micrographs of single crystal InP prepared by photochemical etching. a) Bright field micrograph. b) Selected area electron diffraction pattern illustrating that the edge of the thin region is amorphous. c) Convergent beam electron diffraction pattern of the region adjacent to the amorphous area showing no signs of preparation induced structural artifacts. 92

Fig. 7.4 InP single crystal photochemically thinned. a) Bright field micrograph showing structure of a surface prepared by polishing with 1 μm sized particles. b) Corresponding selected area electron diffraction pattern showing spot splitting indicative of a high degree of crystal damage. 94

Fig. 7.5 Photoluminescence (PL) signal from wafers containing a quaternary layer while being etched. a) A sample with a low signal indicating a thin and/or poor quality layer. b) A sample with a strong signal. c) A sample with a strong signal for which the etching process was terminated in the quaternary layer using computer soft ware. 101

Fig. 8.1 PER versus duty cycle using the AOM at 200 Hz and 20°C. The solid line represents a best fit to the experimental data. The equation is: PER = 20*(duty cycle)$^{(-0.71)}$. 106

Fig. 8.2 PER data obtained with the AOM as predicted by the model of Chapter 3 with a) I=15, k=55, and α=84 and b) I=368, k=145, and α=210. . . . 108

List of Tables

page

Table 2.1 Physical characteristics of n-type InP wafers. 13

Table 3.1 Calculated minimum PER for hole initiation based on constant bulk PER for sample thickness ranging from 30-250 μm, an initiation thickness of 2 μm, and a sample PER of 1.2 μm/min. 31

Table 3.2 Photoetch rate (PER) versus frequency and duty cycle at 35°C and 4.3 mW. 40

Table 5.1 Effective surface area factor (F) with surface preparation. 73

Table 5.2 Effective surface area and photoetch rate for samples prepared with 0.05 and 14.5 μm powders. 75

Table 6.1 Average difference in measured PER between vias produced with one illuminating spot and two illuminating spots on the sample surface. The difference is expressed as a percentage and in all cases the difference is within the experimental scatter of the data. 82

Table 7.1 Uncorrected EDAX data of InP prepared for the TEM with three different methods. The data is expressed as a percentage of total counts found in the window considering only In and P, not the elemental composition. The numbers are an average of at least four samplings. . 96

Chapter 1. Introduction

1.1 Introduction

The work that is reported in this thesis was undertaken to investigate the reliability of 1.3 μm InGaAsP semiconductor diode lasers by examining the microstructure of the devices.

Semiconductor diode lasers are used in the telecommunications industry as the light source in fiber optic networks. The particular lasers of interest are InP based. The composition of the light emitting or active region is $In_{0.73}Ga_{0.27}As_{0.6}P_{0.4}$ with an a band gap of 0.95 eV (1.3 μm). A schematic diagram of a typical diode laser along with an enhanced view of the different epitaxial layers is shown in Fig. 1.1a and b.

A vast amount of time and energy is spent on processing semiconductor wafers into laser devices yet the successful yield is on the order of less than 10%. For economic reasons, the telecommunications industry requires that the lifetime of a laser diode be $>10^5$ hours. As the lasers operate, mechanical stress, local elevated operating temperatures, and current levels act as driving forces causing crystallographic changes, diffusion, and mass transport of the material that

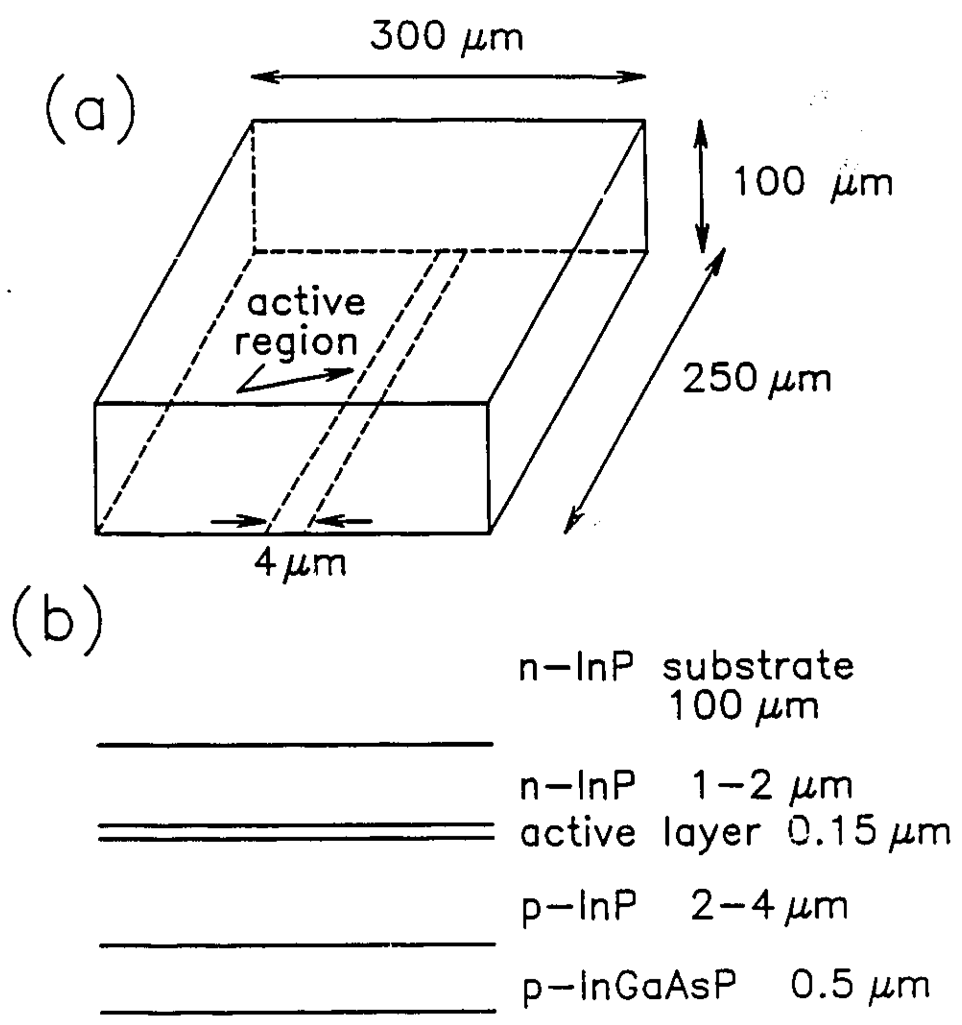

Fig. 1.1 Schematic of a semiconductor diode laser. a) Physical dimensions of the laser and orientation of the light producing active region. b) Typical structure and dimensions of the epitaxial layers that make up a diode laser.

make up the device. Accelerated aging tests and long term operating characteristics have mainly been studied by external monitoring techniques such as photo-, electro-, or cathodoluminescence [1]. Although many modes of degradation have been established from external monitoring, the mechanisms of internal material rearrangement responsible for device failure are not understood [2].

It was the goal of this work to try to provide direct evidence linking degradation mechanisms and changes in the material to device failure by examining and comparing microstructure of good and poor quality devices. The transmission electron microscope (TEM) was the instrument chosen to examine the material. Analytical transmission electron microscopy is capable of providing both structural and chemical information on defect regions in the micron to submicron size range anticipated in this study.

In order to examine samples in the TEM specimens must be thinned to a nominal thickness of 1000 Å but for the best results thinner samples are required. The small physical dimensions of the lasers (100X250X300 μm^3) present a unique problem for sample preparation. However, a new method of specimen preparation was proposed. The method involves photochemical etching. This method was proposed as it is a highly localized process ideally suited for thinning small specimens such as laser diodes.

The driving force for the bulk of the work presented in this thesis was the need to prepare device sized samples for examination in the TEM. Effort was concentrated on the various aspects of the photochemical etching process as it applied to InP. Only after this research had begun was any direct evidence published linking microstructure to device failure [3,4] in InP based lasers. The actual preparation and examination of samples in the TEM became secondary to the study of photochemical etching. However, the technique for TEM sample preparation was successfully demonstrated and evaluated.

1.2 Photochemical Etching of Semiconductors

Photochemical etching and photoelectrochemical etching are techniques for modifying surfaces of semiconductors. Surface modifications include submicron surface gratings [5], grooves [6], mesas [7], waveguides [8], via holes [9], and dislocation identification [10,11]. Modifying semiconductor surfaces with illumination in a reactive environment is controlled corrosion. There are three major cases of light induced corrosion for homogeneous materials illuminated nonuniformly [12]. These are: anodic polarization, also known as photoelectrochemical etching; open

circuit illumination in an indifferent environment; and illumination in a corrosive environment. The environment may be aqueous or gaseous. Production of precise micron or submicron sized features requires the selection of an environment with a low dark etch rate. The open circuit method in an indifferent environment is capable of etch rate sensitivities $>10^4$ without added equipment and difficult processing steps required with anodic polarization experiments. This thesis addresses the open circuit case in an aqueous environment for n-type indium-phosphide (InP).

When a semiconductor is illuminated with light of energy greater than or equal to the band gap, electron hole pairs are created. In n-type material, band bending at the electrolyte/sample interface causes majority carriers (electrons) to travel into the bulk and minority carriers (holes) to the surface. In most semiconductors the corrosion current is limited by the minority carrier concentration [12]. Artificially producing high minority carrier concentrations effectively increases the corrosion current through the minority carrier band. For n-type semiconductors, illuminated regions act as local anodes. Here the material dissolves away with the anodic reaction consuming valence band holes. The anodic reaction is shown in Eq. (1.1):

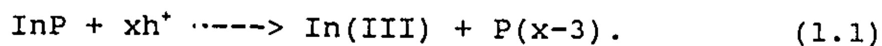

$$InP + xh^{+} \longrightarrow In(III) + P(x-3). \qquad (1.1)$$

Here x is the number of holes required to dissolve one mole of

InP and (x-3) is equal to the oxidation state of phosphorous (III or V) [13].

1.3 Scope and Contents of this Thesis

This thesis reports on the photochemical etching behaviour of n-type InP in an aqueous electrolyte without external biasing. The majority of research on photochemical etching semiconductors has dealt with Si and GaAs in both gaseous environments and aqueous electrolytes [14,15]. Relatively little work has been done on InP in aqueous electrolytes without external biasing.

The most complete work to date on photoetching III-V semiconductors is that of van de Ven and Nabben [16,17]. The first paper [16] uses the concepts of electrochemistry to discuss open circuit photoetching (using GaAs as a model system) as a function of a wide variety of situations including irradiance, wavelength, electrolyte composition and complexing agents, and the ratio of illuminated to dark area. The second paper [17], discusses and defines three kinetic ranges in which photoetching of semiconductors takes place. The three ranges have one of the following as a controlling factor: light intensity, the reduction rate of the oxidizing agent, or the solubility or removal of semiconductor oxidation

products. The paper concludes by discussing some practical aspects of photo induced semiconductor processing. The independent work on InP presented in this thesis agrees well with work presented in the above papers which concentrated on GaAs.

The kinetics of the etching process were investigated by varying the electrolyte pH and temperature along with sample thickness. Other experiments included varying the light level or irradiance and also the frequency and duty cycle of the incident light. The etching process was modelled based on a rate of generation and removal of reaction products. The simple model was capable of predicting the experimental data for duty cycles of 10-100%.

The rate of material removal for n-InP was also found to increase in the presence of low levels of impurity metal ions in solution and/or with gold wire bonds to the surface. Not all metallic impurities exhibited this effect. The reason for the enhanced rate of material removal is believed to be due to the presence of an alternative electron transfer mechanism from the semiconductor to the electrolyte.

The effect of the quality of the semiconductor surface on photochemical etching was also extensively studied. Sample surfaces prepared by chemical and mechanical polishing had different rates of material removal. The removal rates depended upon the size and morphology of the polishing media.

For this work the rate of material removal was limited by the cathodic reaction involving photo generated electrons. Sample surfaces were characterized using transmission and scanning electron microscopy, photoluminescence and mechanical stylus profiling.

The question of local or global saturation of the rate of material removal was also examined. Two via holes were etched simultaneously within a few hundred microns of each other. In tests where two vias were etched, the rate of material removal was the same to within experimental scatter as tests where only one via was etched. This indicated that the material removal rate was not significantly affected by the presence of an additional light source on the sample surface. This is in contrast with earlier work on InP by Willner et al [18]. Willner's group demonstrated that photo induced etching of n-InP was globally saturated when the additional light source was of low irradiance and large area (10 mW/cm^2 and 2 mm in diameter). This set of experiments was undertaken to see if global saturation prevailed with a focussed secondary light source (≈200 W/cm^2 and 40-60 μm in diameter).

A unique application of photochemical etching for the production of vias was developed. Samples were prepared for examination in the transmission electron microscope. This new technique was compared with two traditional sample preparation techniques: ion milling and chemical thinning.

This thesis is divided into eight chapters. Chapter 2 outlines the experimental method and apparatus used throughout the research. In Chapter 3, the photoetching process is studied and modelled as a function of irradiance level and the frequency and duty cycle of the incident light. Chapter 4 shows how and discusses why the rate of material removal changes with certain metal ion impurities in the electrolyte and with gold wire bonds attached to the sample surface. The effects of surface roughness on the rate of material removal is examined in Chapter 5. Chapter 6 addresses the question of local or global saturation of the rate of material removal. The merits of photoetching as a tool for TEM sample preparation are discussed in Chapter 7. Chapter 8 summarizes the thesis and presents some recommendations for future research.

This work is recorded in four manuscripts and one conference proceedings, of which two have been published [19,20] and three have been submitted for publication [21,22,23].

Chapter 2. Experimental Method and Apparatus

2.1 Introduction

The basic chemistry of photochemical etching is understood and was outlined in Chapter 1. However, there remain many unanswered questions regarding the photochemical etching behaviour of InP. Photochemical etching properties of InP have been limited to wavelength, irradiance and electrolyte studies [6,7,24].

Although many types of surface modifications have been demonstrated, the mode of surface modification adopted for study in this project was the production of vias. This mode of surface modification was chosen because of the potential to produce specimens for the TEM and it was straight forward to determine the etching rate by monitoring the light level transmitted through the sample.

To understand the etching process and to optimize the photoetching process for TEM sample preparation, a wide range of experimental situations such as sample thickness, surface preparation, electrolyte temperature, impurities, and pH, and illumination irradiance level, duty cycle, and frequency were investigated.

The remaining contents of this chapter discuss the experimental method and apparatus used in the production of vias and of samples for the TEM. Outlined specifically are the details of sample surface preparation prior to photochemical etching, sample preparation for the TEM by traditional methods (ion milling and chemical thinning), and the method and apparatus used in the photochemical etching experiments.

Although other pieces of equipment and techniques were used as diagnostic tools (i.e., electron microscopes and photoluminescence) the standard technical details of their operation are not outlined. However, relevant information regarding the conditions of operation is specified as required.

2.2 Sample Preparation

Three cases of sample preparation are described. Outlined first is the preparation of surfaces prior to photochemical etching for the production of vias. The other areas outlined are the preparation of cross sectional and plan view samples for the TEM by ion milling and chemical thinning.

2.2.1 Surface Preparation for Photochemical Etching

The material used was substrate quality InP wafers purchased from Sumitomo Electric Limited. Four wafers in total were purchased, two at a time. The wafer specifications are listed in Table 2.1. Due to the large sample thickness it was necessary to thin the wafers. This was done in two ways: chemical thinning using a solution of bromine in methanol 1% by volume (Br:MeOH) or mechanical polishing using a lapping wheel and various sized abrasives.

Chemical thinning was performed in a fumehood by lightly rubbing the sample face down on a smooth saturated cotton polishing cloth mounted on a glass plate. When the sample was adequately thinned it was quenched in methanol to prevent the smooth mirror finish from becoming black in colour with a matte finish. Mechanical polishing was performed by fastening the sample onto a flat metal block with a low melting point (≈80°C) clear wax known as crystal bond. The sample and block were thoroughly cleaned using a cotton swab with water, then rinsed in methanol and dried with compressed air. The samples were polished using new cotton polishing cloths starting with 14.5 μm followed by 5.0, 1.0, 0.3, and 0.05 μm alumina powders suspended in deionized water (resistivity ≈18 MΩ-cm). Care was taken to clean the sample and block between polishing stages to minimize the transfer of large

Table 2.1 Physical characteristics of n-type InP wafers.

	Wafers 1 and 2	Wafers 3 and 4
Thickness	380±5 μm	350±5 μm
Doping density (n)	$6.5 \pm 0.1 X 10^{18}$ cm^{-3}	$5.7 \pm 0.1 X 10^{18}$ cm^{-3}
Dopant	Sulphur	Sulphur
Etch pit density	$\leq 5.0 X 10^{3}$ cm^{-2}	$\leq 5.0 X 10^{3}$ cm^{-2}
Mobility	$1.35 X 10^{3}$ $cm^{2}/(Vs)$	$1.3 X 10^{3}$ $cm^{2}/(Vs)$
Surface preparation	as cut brief etch	1 as cut,1 polished

particles onto cloths intended for smaller powders. Samples were polished for at least 15 minutes at each polishing stage.

The 14.5 and 5.0 μm powders were grey while the 1.0, 0.3, and 0.05 μm powders were white in colour. All powders had the hexagonal structure with a hardness of 9 on the Mohs scale, except the 0.05 μm powder which was cubic with a hardness value of 8. All powders were purchased from Buehler Limited. In some preliminary work diamond paste was used instead of alumina powders.

After thinning, the samples were removed from the polishing block, cleaned in acetone, methanol, and deionized water. Samples were stored in individual plastic petri dishes in room air.

2.2.2 Sample Preparation by Ion Milling

As mentioned in Chapter 1, photochemical etching was used to prepare specimens for the TEM. In an effort to evaluate this method, samples were also prepared using traditional techniques. One of the more widely used methods of semiconductor sample preparation for the TEM is ion milling. Samples were prepared in both plan view and cross sectional configuration. Both sample types were prepared in a similar manner with the exception of the starting material.

For plan view samples the starting material was thinned to approximately 150 μm in thickness. For cross sectional samples the starting material was constructed to take on the form of a stack or raft. Pieces greater than or equal to 3 mm in length and greater than ≈300 μm wide were cleaved from the host piece. The pieces were then glued together with a conductive epoxy (epo-tek H20E from Epoxy Technology Inc.) by stacking them one on top of each other until they reached 3 mm in height. After the epoxy cured the stack was turned on its side and thinned on both sides resulting in a parallel sided structure ≈150 μm in thickness.

The following procedures were carried out for both sample configurations. First, 3 mm disks were cut out using a Gatan ultrasonic disk cutter. The disk dimension was dictated by the TEM sample holder. The disks were thinned on both sides using a Gatan dimple grinder to a central thickness of ≈50 μm in two steps. The samples were initially thinned using 3.0 μm diamond paste and then buffed to a smooth mirror finish using 1.0 μm diamond paste. The buffing was necessary to avoid preferential crystallographic thinning during ion milling. Dimpled samples were then transferred to a Gatan Model 600 ion milling machine. The sample stage was rotated and set at a 12° tilt. Argon gas was used as the ion source and the guns were operated at 4 kV with a gun current of 0.5 mA total. The specimen current was ≈20 μA. The samples were ion milled at

liquid nitrogen temperature. This was necessary to avoid preparation artifacts as were found on samples ion milled at room temperature. The thinning process was automatically terminated when light from a 1 mW HeNe laser was detected as it passed through the sample.

2.2.3 Sample Preparation by Chemical Thinning

Chemical thinning is one other widely used method for TEM sample preparation for semiconductors. Highly sophisticated commercial systems are available, however, a comparatively rudimentary but effective homemade system was used. The apparatus consisted of a tapered plastic flask with an opening in the bottom. The thinning chemical flowed out of the flask through an inert tube where it impinged on the sample. Both one and two sided thinning was performed. The thinning process was stopped when light was detected through the sample with the naked eye. A solution of 1% bromine in methanol by volume was used as the thinning agent. The samples were immediately quenched in methanol after thinning to prevent excessive thinning, blackening, and surface roughening.

2.3 Method and Apparatus for the Production of Vias

The experimental apparatus for the production of vias is shown schematically in Fig. 2.1. A Cyonics 4.3 mW Ar^+ laser at 488 nm or a Cyonics multiline Ar^+ laser at 10.0 mW was used as the light source. The light was focused onto the sample through a 2.5X objective lens (NA=0.10) mounted on a micrometer stage resulting in an irradiance of ≈200-250 W/cm^2 at the sample surface. The spot size of the beam which was reflected from the sample surface was minimized to obtain a proper focus. The fluid height was periodically monitored and kept constant to ensure no change in focus as fluid evaporated with time. Evaporation was a problem particularly during elevated temperature experiments as changes in focal length with fluid height produced different sized vias with different etch rates. Fluid height maintenance was accomplished by measuring the potential drop across a resistor in series with two copper probes. One probe was completely immersed in the electrolyte, while the other was positioned at the desired height of the electrolyte. If the potential across the resistor was zero, indicating an open circuit and thus that the fluid was not in contact with the copper probes, a one way gate valve was opened introducing fresh electrolyte into the system. The valve was closed when a non-zero potential was measured indicating that the probes were in contact with the

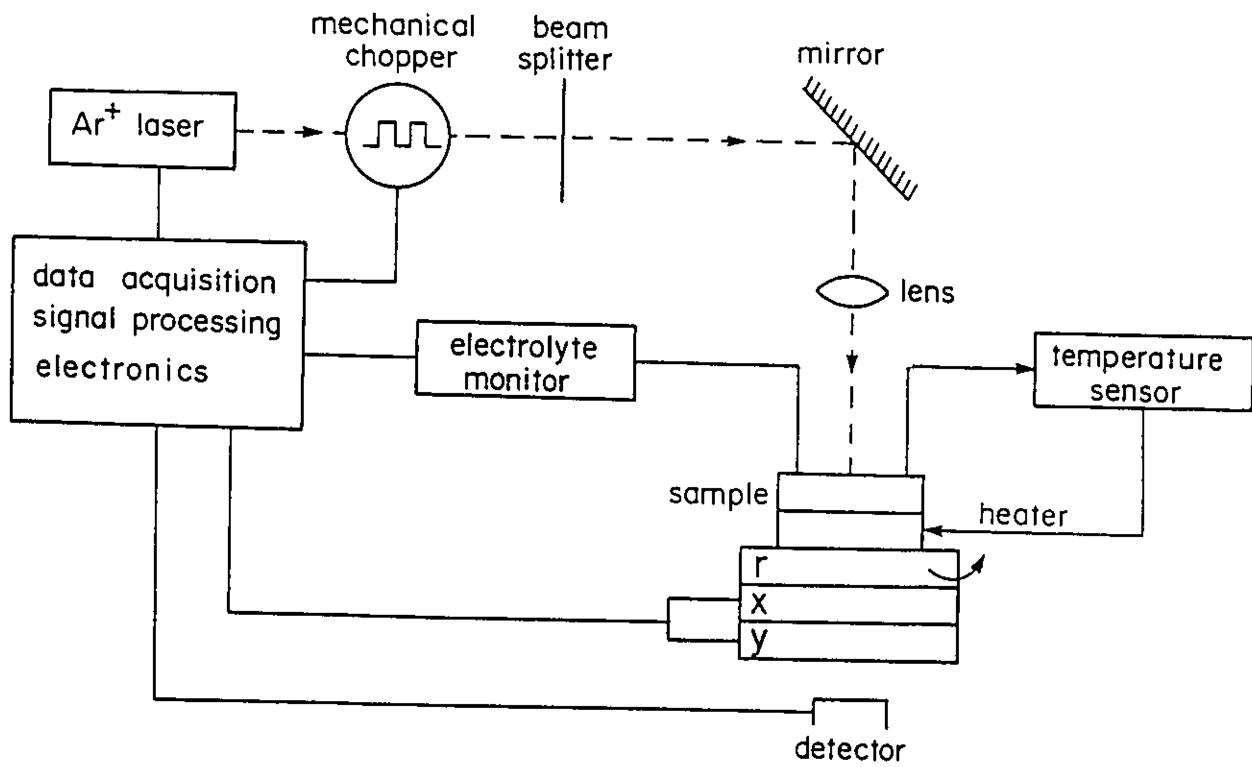

Fig. 2.1 Schematic of the experimental apparatus for via production.

electrolyte, and the fluid height was properly adjusted.

Prior to photochemical etching, samples approximately 1.0X0.8 mm^2 in surface area were cleaved from the larger polished pieces. They were then cleaned in acetone, methanol, and deionized water baths and mounted in a glass petri dish polished side up with crystal bond. A fresh solution of H_3PO_4 (85%) in de-ionized water 1:9 by volume was normally used as the electrolyte.

The petri dish was mounted on a rotation stage which was placed on a computer controlled x-y translation stage equipped with optical encoder micrometers capable of micron precision positioning. Etch rate data was obtained by knowing the sample thickness and time taken for sample perforation. Sample thickness was measured with a Sony electronic micrometer. An accurate estimate of the time taken to perforate the sample was determined by monitoring transmitted light with a silicon or InGaAs photodiode. For duty cycles other than 100%, the transmitted signal was detected by mechanically chopping the light and using a lock in amplifier. The frequency of chopped light was varied from 15 Hz to 3.2 kHz and the duty cycle was varied from 5% to 100% using a mechanical chopper. Duty cycle is defined as the ratio of time the light is on, to time on plus time off. For duty cycles below 5% an acousto optic modulator (AOM) was used. The modulator was a TeO_2 crystal which when activated

diffracted the incident laser beam from its original path. The crystal was driven using a Wavetech pulse generator. The crystal had a rise time on the order of 100 ns. This allowed for light pulses of ≥1 μs duration to be used without the need to correct for rise/fall time effects. Thus, at a frequency of 200 Hz, the lowest duty cycle was 0.02%.

An example of the waveform from the acousto optic modulator with a 1 μs on time is shown in Fig. 2.2. The signal was that of the first order diffracted beam as detected with a silicon photo detector. The output signal of the modulator closely followed the input signal. The desired 1 μs pulse was not significantly limited by the crystal rise time.

Sample temperature was monitored by placing a type J (iron-constantan) polyethylene coated thermocouple in the electrolyte within 1 cm of the sample. An Omega 4001 temperature controller was used to display the temperature and control a resistive heater beneath the petri dish. Sample temperature ranged from 20°C to 50°C and was controlled to ±1°C.

An example of the data obtained with the apparatus is shown in Fig. 2.3. Shown is the detector signal as a function of illuminated time for a sample 127 μm thick etched at 20°C, 4.3 mW incident power with a 50% duty cycle. Hence, total elapsed time is twice the illuminated time. The abrupt change in detector signal indicated that the sample had become

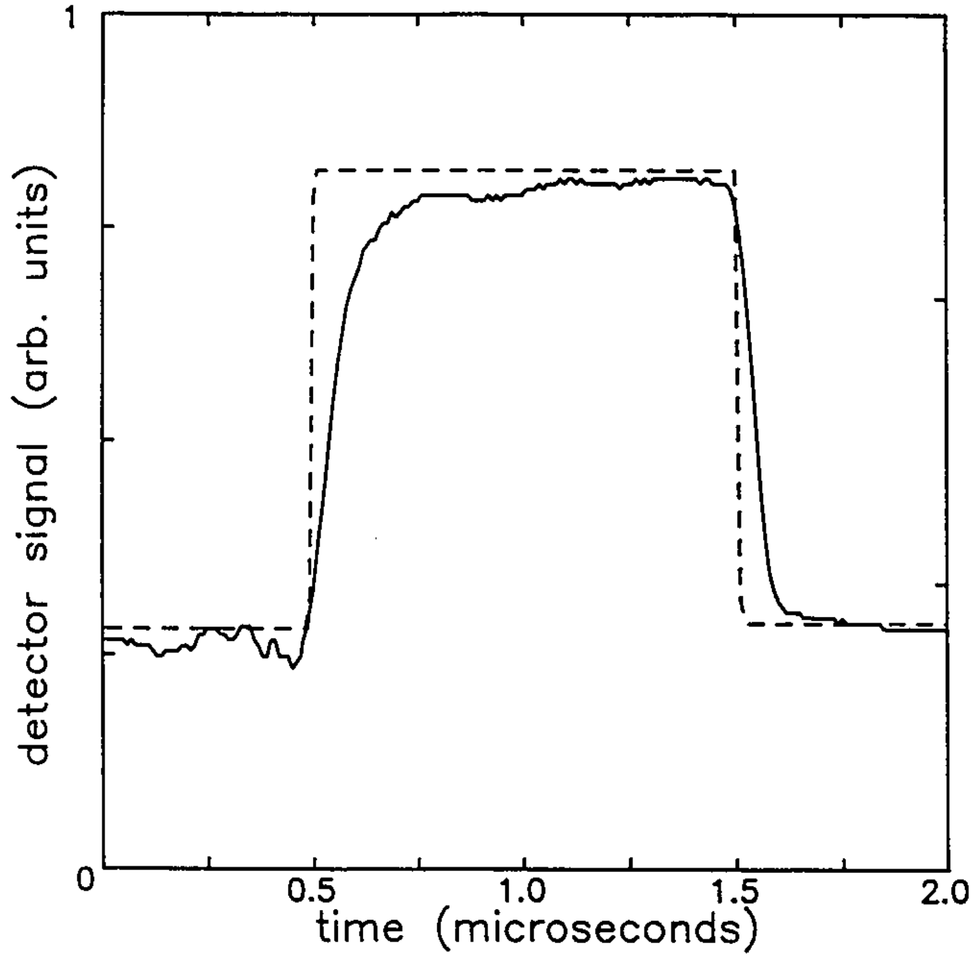

Fig. 2.2 Rise time of the acousto optic modulator (AOM). The broken line corresponds to the desired wave form sent to the AOM and the solid line represents the measured light output from the AOM using a silicon detector.

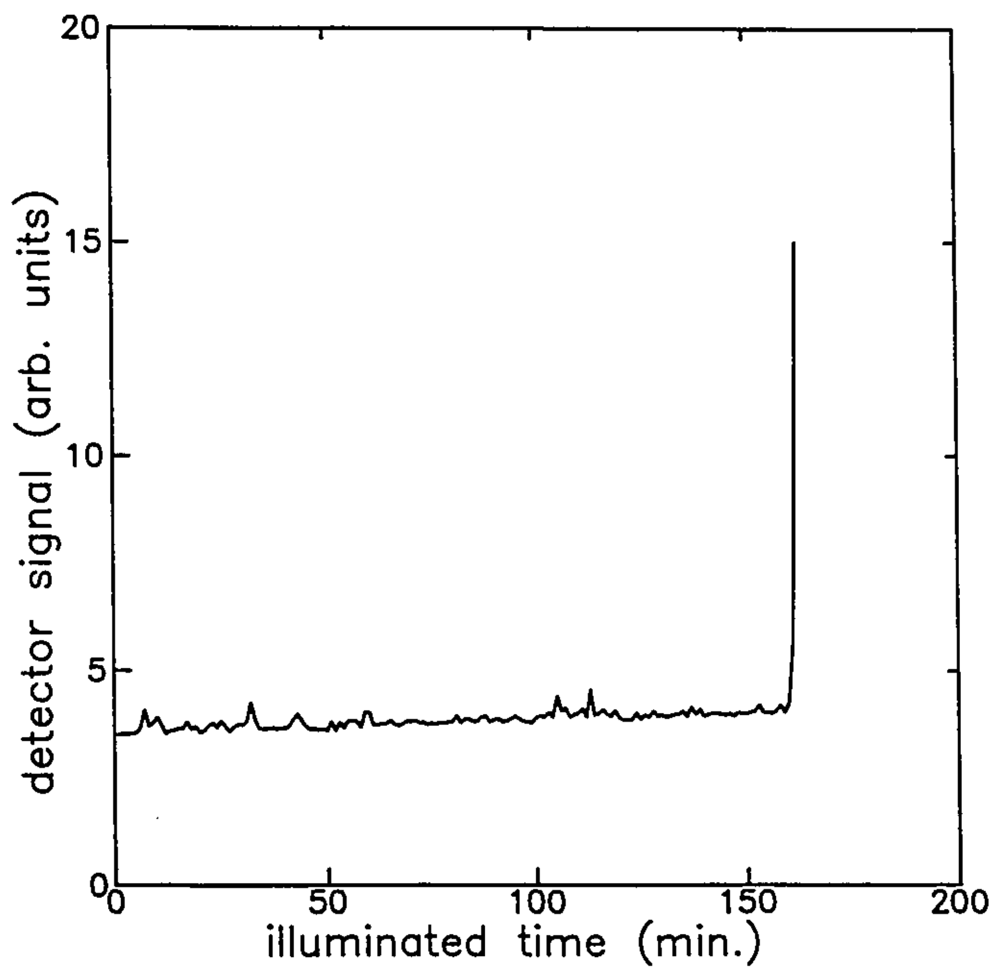

Fig. 2.3 Typical data showing detector signal versus illumination time for an etched via.

perforated. In this work the rate of material removal is quoted as the photoetch rate (PER). The PER is defined as the etch rate divided by the fraction of time the illumination is on. PER is therefore an average etch rate constant in time.

Another set of experiments was undertaken to isolate the active region of a semiconductor wafer for examination in the TEM by photochemical etching. These experiments were performed on unprocessed InP wafers with various layers epitaxially grown on them. The layer of interest was the active layer, this is the layer that emits light in semiconductor laser diodes. The composition of the active layer was $In_{0.73}Ga_{0.27}As_{0.6}P_{0.4}$ with a band gap of 1.3 μm. The InP wafers were photochemically etched from the substrate side down to the epi-layer side. When the incident light from the Ar^+ laser reached the active layer (indicating that the via bottom was at the active layer), photoluminescence (PL) corresponding to the wavelength of the active layer was produced. When PL of this wavelength was detected the etching process was terminated and the sample was ready for TEM evaluation. The PL from the active region was detected by replacing the silicon photo detector with an InGaAs photo detector, eliminating the infrared light from the Ar^+ laser before etching by using a Melles Griot 03MCS005 cold mirror, and eliminating all stray light from the surroundings and the Ar^+ laser with an Oriel 0-42038 optical filter allowing only

light 1.2-1.4 μm in wavelength to pass into the detector. The results of these experiments are discussed in Chapter 7.

2.4 Summary

The experimental method and apparatus for the preparation of samples for the TEM using photochemical etching and traditional techniques were outlined. The remaining chapters focus on the factors controlling the photochemical etching process. The technique as a tool for TEM sample preparation is also evaluated in a later chapter.

Chapter 3. Photoetch Rate as a Function of Temperature and Illumination

3.1 Introduction

Etching experiments consisted of focusing light onto a sample to produce an etched via through the sample. In the irradiance (power/unit area) range used ($\approx$200-250 W/cm^2 peak level of chopped light), laser induced temperature rise is negligible [25,26] and etching proceeds non-thermally with light generated carriers [8]. Vias result from a self propagating vertical waveguide. The etched profile begins by assuming the same shape (Gaussian) as the beam intensity distribution. As time progresses, the etched profile becomes tubular with near vertical walls due to internal reflections of the incident light [27]. A typical intermediate profile is shown in Fig. 3.1. The etch rate data presented herein were calculated using the total illuminated time taken to perforate a sample of known thickness with a via or hole not total time elapsed until perforation. The presented data is therefore quoted as photoetch rate (PER). Since etching takes place as a result of the illumination, presenting the data in this way is accurate, representative of the process, and helps

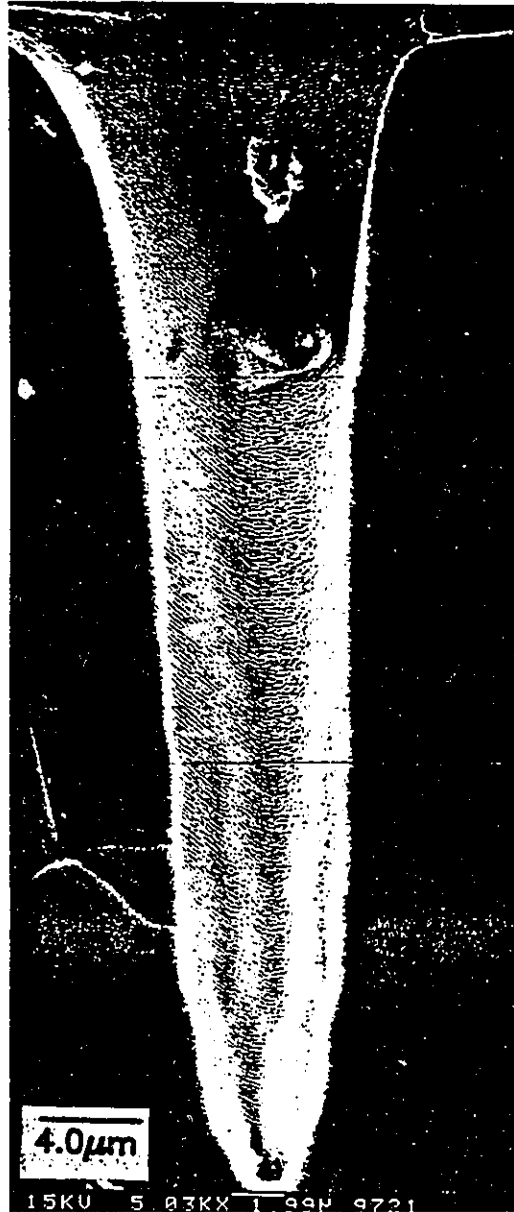

Fig. 3.1 Cleaved cross section of an etched via showing the self propagating waveguide.

to understand the dependence of the etch rate on illumination duty cycle and frequency. Each data point represents an average of 4-10 etched holes from one sample taken from a common wafer. Error bars in all figures represent plus and minus one standard deviation of the mean. The holes were etched in succession with the electrolyte level kept constant unless otherwise indicated. Addition of fresh electrolyte stirred the solution but did not appreciably alter the solution temperature due to the small volumes added.

3.2 Determination of Photoetching Control

The experiments and the corresponding data reported in this section were undertaken to try to determine if the photoetching process was diffusion limited or reaction rate limited.

The thickness of wafers that were etched varied from approximately 30 μm to over 200 μm. Fig. 3.2 shows that etch depth appears to depend linearly on etching time. This indicates that concentration effects at the bottom of the hole during the etching process was not a significant problem. Such a problem would show that thicker samples would have a lower PER than thinner samples as the conditions at the hole bottom result in a decreased etching ability due to

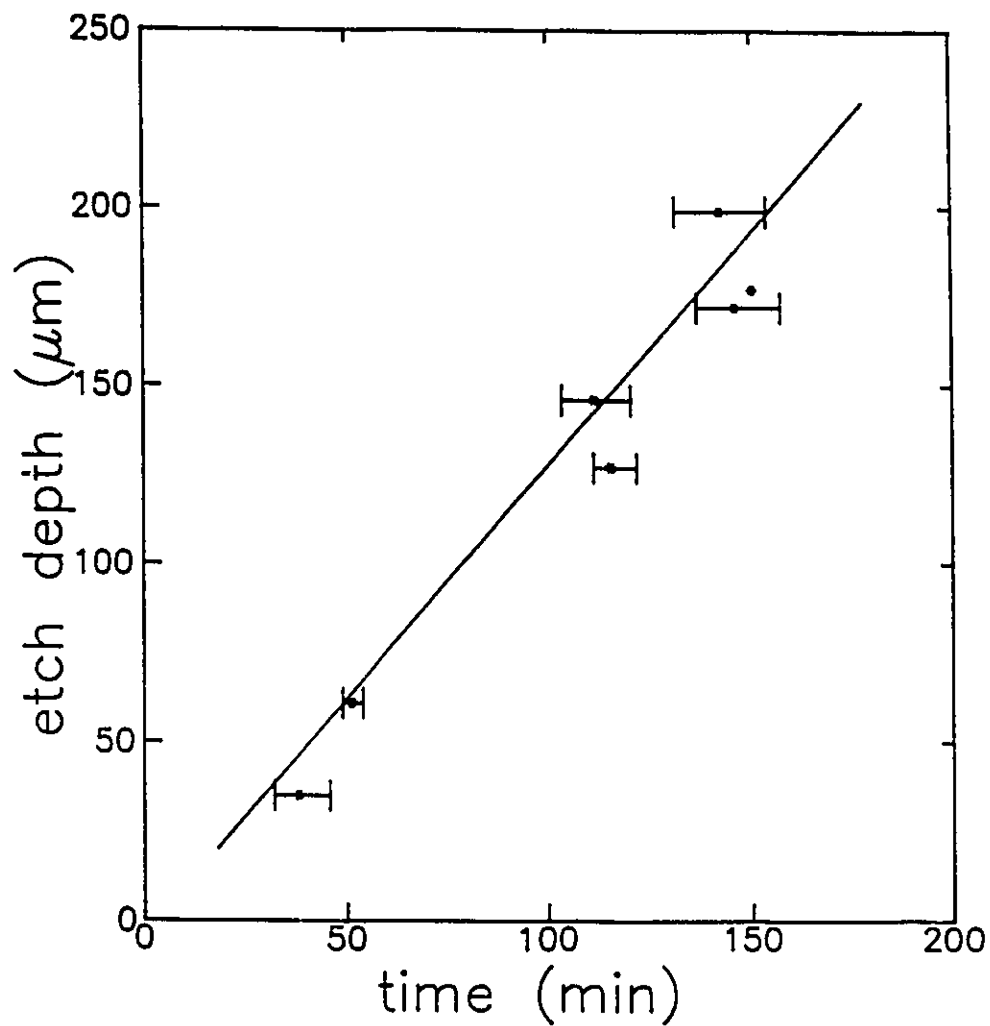

Fig. 3.2 Photoetch depth versus time at 20°C, 200 Hz, and 50% duty cycle.

concentration effects.

The data also indicate that the etching process does not appear to be dominated by a lengthy initiation period due to the semiconductor surface as the line in Fig. 3.2 passes through zero depth at zero time.

The etching process may be viewed as a two staged process. Stage one is an initiation stage and has a PER associated with it. Stage two etching is etching of the bulk material. The PER may be expressed as,

$$PER=(th_i + th_b)/(t_i + t_b), \quad (3.1)$$

where th is thickness, t is time and the subscripts i and b are for the initiation stage and bulk stage respectively.

The overall PER is equal to 1.2±0.1 μm/min for all thickness values. The PER for hole initiation was measured with a mechanical stylus profiler after etching for 20 minutes with a 50% duty cycle. This time interval was chosen so that the amount of material removed was significant enough to be measured accurately. The initiation PER was 0.72±0.25 μm/min. The large variation is attributed to the inhomogeneous sample surface produced by mechanical polishing. This PER is significantly lower than the overall PER of 1.2±0.1 μm/min, yet no significant variation of overall PER with sample thickness was observed.

The minimum PER for initiation without significantly affecting the overall average PER was estimated using

Eq. (3.1) as follows. It is known that the PER is equal to 1.2 μm/min and the bulk PER (th_b/t_b) is the same (to within experimental error) for all samples regardless of thickness. To start, various values of PER for initiation, and bulk thickness were assumed. The corresponding initiation and bulk etching times were calculated and finally the bulk PER was obtained. The PER for initiation was accepted as a possible rate only if the bulk PER was within ±5% for all values of thickness. The data was calculated by assuming an initiation thickness of 2 μm (based on results of dislocation depth reported in Chapter 5). The PER for initiation was varied from 0.1-1.2 μm/min, and the bulk thickness was varied from 30-250 μm. Table 3.1 shows that the minimum value of PER for initiation is 0.67 μm/min while maintaining a constant bulk PER and an overall PER of 1.2 μm/min. The simple model is consistent with the data and it also predicts that the minimum PER for initiation decreases with decreasing initiation thickness.

Although the line in Fig 3.2 appeared to be linear and pass through zero depth at zero time it is known that the surfaces are highly imperfect. Therefore, it was expected that there should be a lower PER for the initial stages of hole formation. The purpose of the above exercise was to demonstrate that there may be a lower PER associated with initiation, however, it was not low enough to significantly

Table 3.1 Calculated minimum PER for hole initiation based on constant bulk PER for sample thickness ranging from 30-250 μm, an initiation thickness of 2 μm, and a sample PER of 1.2 μm/min.

PER_i (μm/min)	PER_b (μm/min)	
	30 μm	250 μm
0.10	4.498	1.316
0.15	2.249	1.271
0.20	1.800	1.250
0.25	1.607	1.238
0.30	1.500	1.230
0.35	1.432	1.224
0.40	1.384	1.220
0.45	1.350	1.216
0.50	1.323	1.214
0.55	1.303	1.211
0.60	1.285	1.210
0.65	1.272	1.208
0.67	1.267	1.207
0.80	1.241	1.205
1.20	1.200	1.200

affect the overall average PER.

To estimate the effects of electrolyte enrichment and/or extended electrolyte exposure, the dark etch rate and pH dependency were investigated. At room temperature the dark etch rate, as measured with a mechanical stylus profiler, was ≤1.0 Å/min at 20°C over 24 hours, and ≤2.5 Å/min at 50°C over 6.5 hours. Also, dark and PERs were not significantly affected (<5% difference) by solution pH over the range 2.3 to 1.6 or 1:24 to 1:4 H_3PO_4:H_2O by volume.

PER versus temperature studies revealed that the PER increased almost four fold from 1.2±0.1 to 4.1±0.3 μm/min by increasing the temperature from 20°C to 50°C for a 50% duty cycle. Duty cycle is defined as the ratio of time the light is on to time on plus time off. An Arrhenius treatment, shown in Fig. 3.3, indicated that the process was thermally activated with an activation energy of 0.34±0.03 eV. However, the activation energy as found by fitting to the rate equation model (section 3.3), for samples etched with illumination corresponding to the saturation level of irradiance for all temperatures is 0.50±0.05 eV. This arises from the dependence of irradiance saturation level on temperature and is discussed in greater detail in section 3.3.

The increased PER at elevated temperature was at the expense of hole quality. Fig. 3.4 compares two vias produced at 20°C and 50°C. At higher temperatures the normally sharp

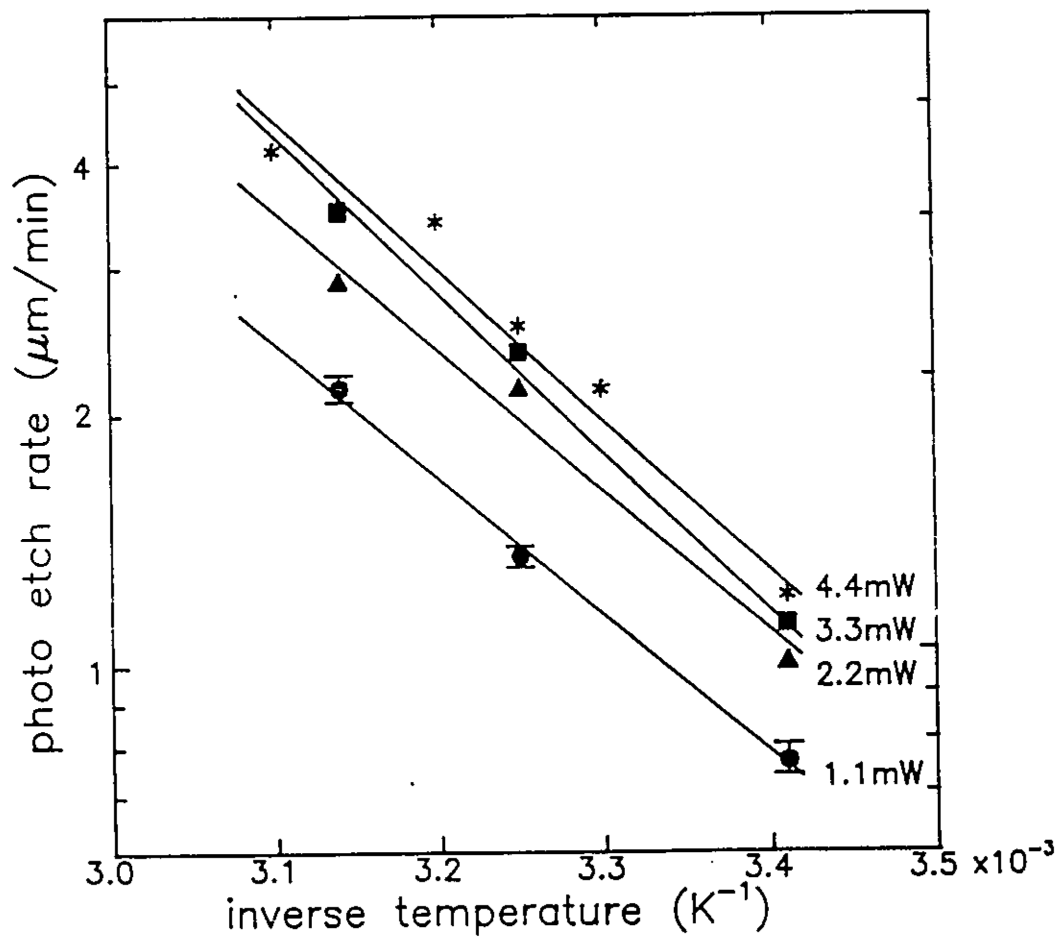

Fig. 3.3 Photoetch rate versus inverse temperature at constant irradiance, 200 Hz, and 50% duty cycle.

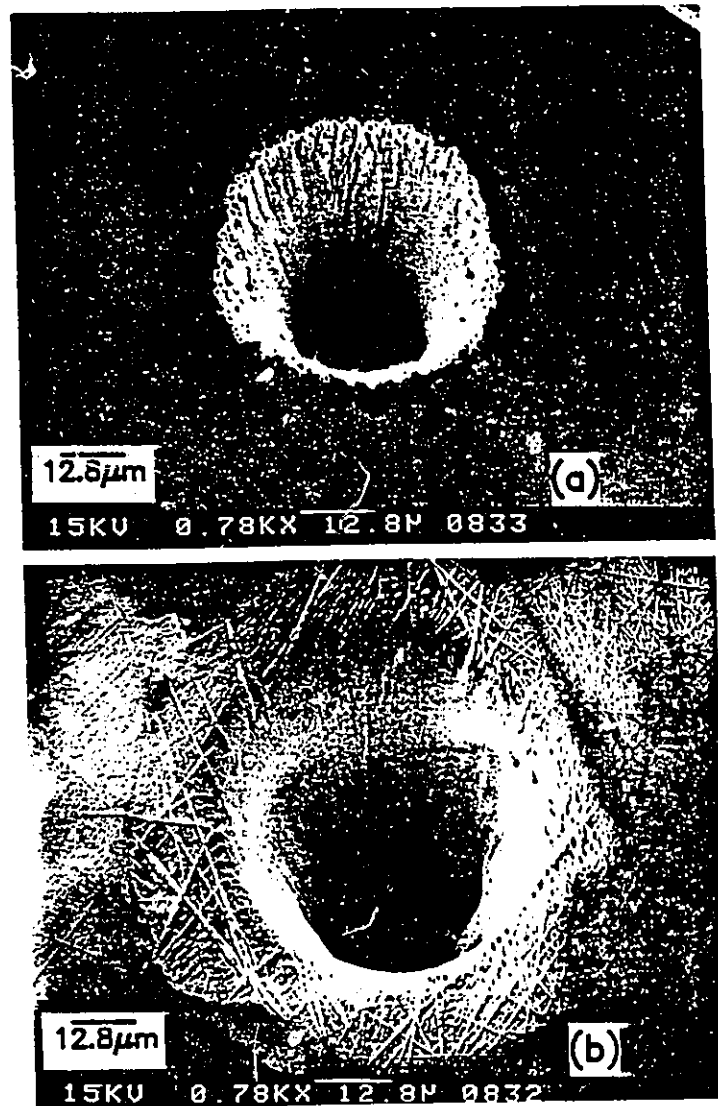

Fig. 3.4 Top view of two vias etched at a) 20°C and b) 50°C.

edges have eroded significantly due to increased sensitivity to photoetching. Low light levels at the hole periphery also amplify the presence of defects stressing the need for high surface quality prior to etching.

It is well known that dissolution depth of a solid that varies linearly with time is reaction rate limited, whereas a $t^{1/2}$ dependence indicates a diffusion controlled reaction [28]. Also, diffusion controlled reaction rates increase with the concentration of reacting species and solution stirring [29,30]. Studies on GaAs dissolution in sulphuric acid solutions [31] report thermal activation energies of 6-8 kcal/mol (0.26-0.34 eV) for diffusion control and 8-11 kcal/mol (0.34-0.48 eV) for reaction rate control. The data outlined above and presented in Figs. 3.2 and 3.3 show a linear photoetch depth dependence with time, and a thermal activation energy (including the temperature dependence of the saturation level) of $\geq 0.34 \pm 0.03$ eV. This, coupled with the observations that pH and stirring had little affect on PER, indicates that under these experimental conditions the process is reaction rate controlled.

3.3 Illumination Effects on Photoetch Rate

The relationship between PER and irradiance at various

temperatures is shown in Fig. 3.5. Irradiance was calculated using a 40 μm beam diameter based on average via diameters observed in the scanning electron microscope, and 30% total reflection loss due to the air/liquid and liquid/sample interfaces. The curves show an initial rapidly increasing region at low irradiance tending towards a plateau or saturation level where PER increases slowly with irradiance. These results are consistent with data reported for GaAs and InP in various electrolytes at comparable power levels [24].

PER data and hole quality were strongly dependent upon surface quality prior to etching. Surface contamination affects absorption while surface defects act as recombination centres [32]. Polishing scratches resulted in etch resistant regions presumably because photo induced carriers recombine at defects, while microscopic pits appeared to act as miniature waveguides producing "satellite" vias as shown in Fig. 3.6.

In preliminary experiments it was observed that for a given sample, the PER was different for continuous illumination and mechanically chopped illumination. In both cases the etch rates are reported as PER. That is the total time the sample was illuminated, not total time elapsed until perforation, although, for continuous illumination there is no difference. The dependence of PER on frequency of chopped light and duty cycle was investigated and is presented in

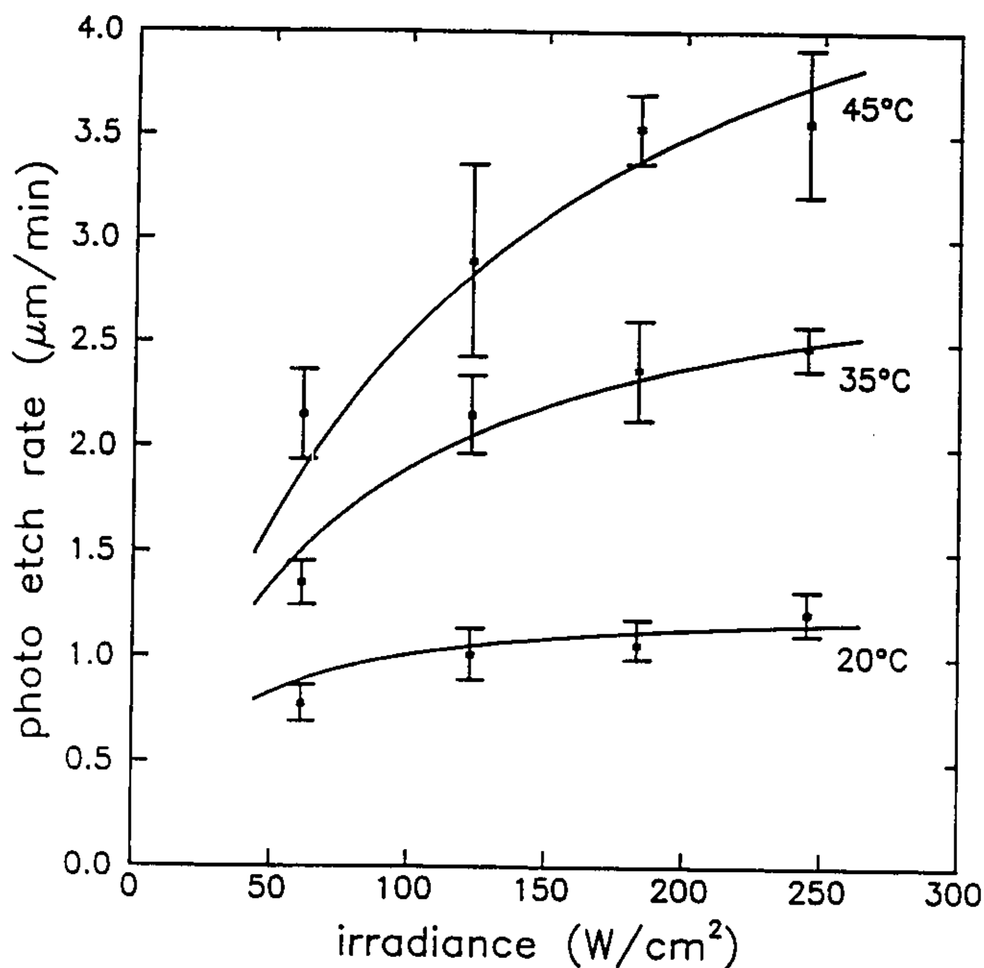

Fig. 3.5 Photoetch rate versus irradiance at 200 Hz, and 50% duty cycle. Solid lines represent predicted behaviour using model superimposed on experimental data where α=84, and k=255, 140, and 55 for 45°C, 35°C, and 20°C respectively. The symbols α and k are discussed in the text.

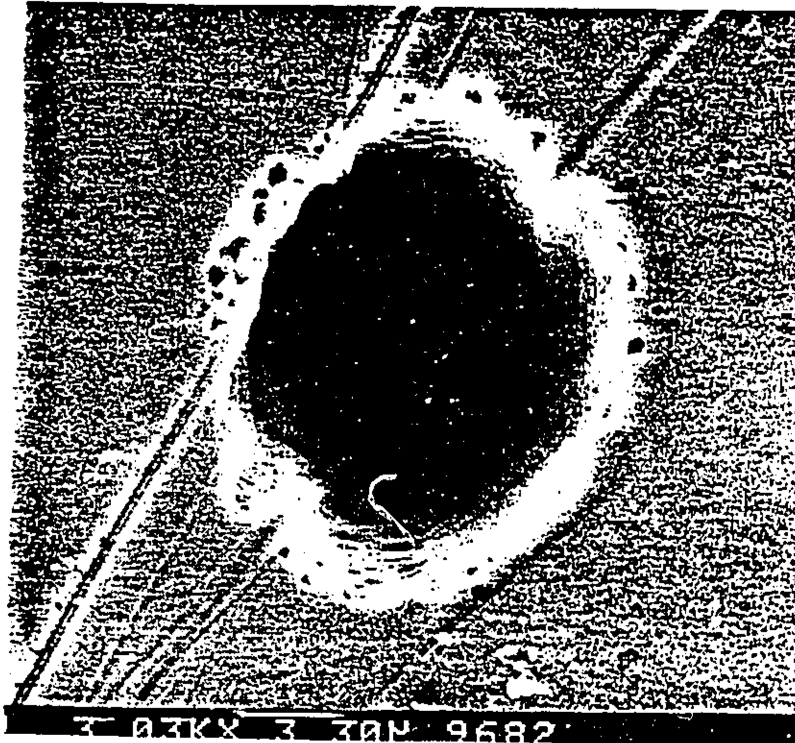

Fig. 3.6 Top view of an etched via highlighting features produced by defects. Note the resistance to etching at polishing scratches presumably due to carrier recombination, and small satellite vias around the perimeter believed to be caused by microscopic waveguiding.

Table 3.2 and Fig. 3.7. Frequency of chopped light had little or no affect on PER over the range 100 Hz to 3.2 kHz. Duty cycle, however, significantly affected the PER. For example, using a 5% duty cycle, the PER was an order of magnitude larger than that with continuous illumination (100% duty cycle) while the total elapsed time to perforation was only twice as long.

A rate equation model based on a simplified picture of the etching process was developed. In the model it is assumed that the rate of generation of oxidized material depends on the local light intensity and the number of photo generated holes. Upon illumination, a monolayer of reactants forms on the surface as photo generated holes are rapidly consumed. This monolayer must be removed for further etching to proceed. Removal of the reaction products is believed to be the rate determining step. Reaction products are assumed to be generated only during the illumination portion of the cycle, while material removal is assumed to be continuous. The rate of removal of material, R, is given by:

$$R = k\theta, \qquad (3.2)$$

where θ represents the fraction of illuminated surface covered by reaction products, and k is the rate constant for removal of material. The rate of generation of reaction products, G(t), is taken to be the product of irradiance, I(t), and the fraction of surface area not yet covered with reaction

Table 3.2 Photoetch rate (PER) versus frequency and duty cycle at 35°C and 4.3 mW.

	10% duty cycle				50% duty cycle			
Frequency (Hz)	100	200	400	800	100	200	1000	3200
PER (μm/min)	7.29 ±0.2	7.37 ±1.0	7.49 ±0.7	7.07 --	2.25 ±0.2	2.51 ±0.3	2.51 ±0.4	2.75 ±0.3

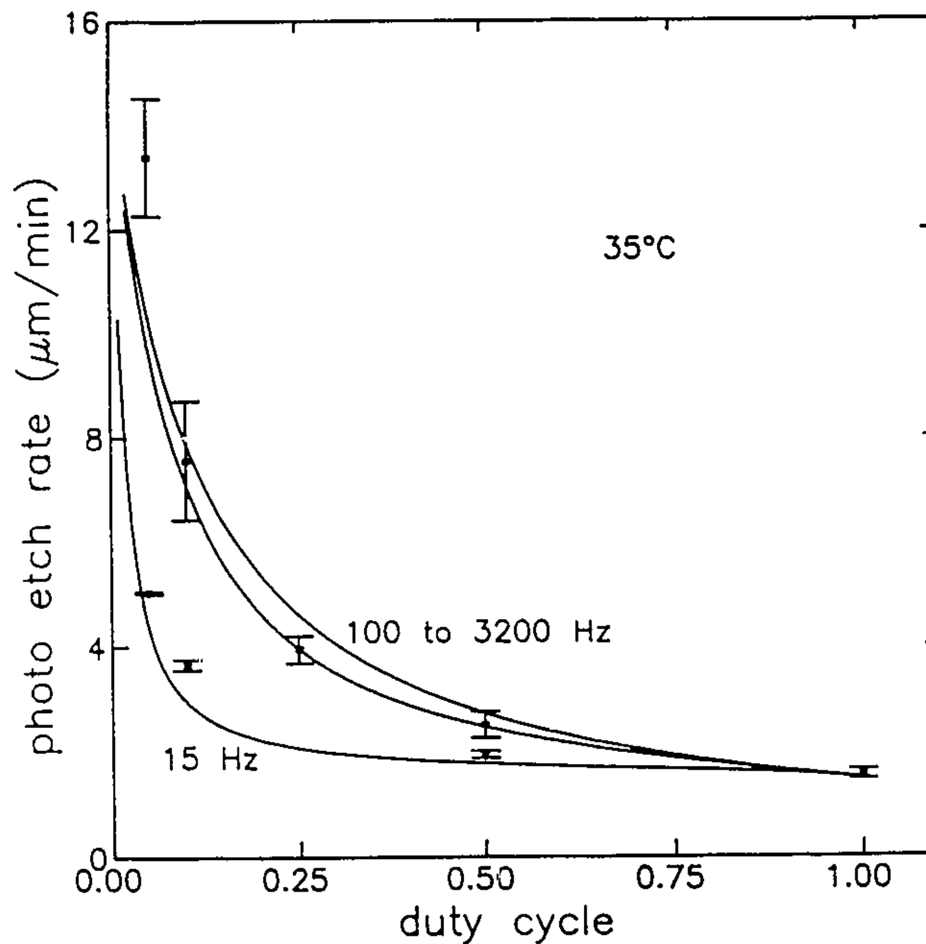

Fig. 3.7 Photoetch rate versus duty cycle at 35°C. Data is for 200 Hz and 15 Hz. Solid lines represent behaviour for 15, 100, and 3200 Hz where $\alpha=84$, $k=140$, and $I=15$. The symbols α, k, and I are discussed in the text.

products:

$$G(t) = (1-\alpha\theta)I(t). \tag{3.3}$$

The term α is introduced as a surface coverage enhancement factor. It is a fitting parameter which may account for regions where photo induced carriers do not react due to recombination at defect sites or regions already covered with reaction product. The time rate of change of surface coverage is given by:

$$d\theta/dt = G(t)-R = (1-\alpha\theta)I(t)-k\theta. \tag{3.4}$$

Eq. (3.4) must be solved to obtain the rate of removal of material R. In the experiments the argon ion light was mechanically chopped and thus $I(t)=I$ for t_{on} seconds and $I(t)=0$ for t_{off} seconds each cycle. With these definitions the chopper frequency (f) is $(t_{on}+t_{off})^{-1}$ and the duty cycle (dc) is $t_{on}/(t_{on}+t_{off})$. An expression for the etch rate in terms of the variables of Eq. (3.4) and t_{on} and t_{off} is obtained by recognizing that $\theta(t=0)=\theta(t=t_{on}+t_{off})$ due to the periodic nature of the chopping process. The photoetch rate R_{ph} equals the time averaged value of the rate of removal of material divided by the fraction of time that the light is illuminating the semiconductor, i.e.,

$$R_{ph} = \langle k\theta\rangle(t_{on}+t_{off})/t_{on} \tag{3.5}$$

$$= \left(\frac{kI}{k+\alpha I}\right) + \left(\frac{1}{t_{on}}\right)\left(\frac{\alpha I^2}{(k+\alpha I)^2}\right)\left(\frac{1}{\coth[(kt_{off})/2]+\coth[(k+\alpha I)t_{on}/2]}\right).$$

Eq. (3.5) predicts that the PER is an increasing function of

the irradiance for small values of I and saturates for large values of I. It also predicts that the PER is a function of frequency as t_{on}=dc/f. In the limit kt_{off}<<1, and large $(k+\alpha I)t_{on}$, Eq. (3.5) becomes:

$$R_{ph} = \left(\frac{kI}{k+\alpha I}\right)+\left(\frac{kt_{off}}{2t_{on}}\right)\left(\frac{\alpha I^2}{(k+\alpha I)^2}\right). \quad (3.6)$$

Eq. (3.6) predicts that R_{ph} is independent of frequency as t_{off}/t_{on} is constant for all frequencies for a given duty cycle. The predicted photoetching behaviour can be seen in Figs. 3.5 and 3.7. The data is represented by symbols and accompanying error bars, while the lines represent predicted R_{ph} values. The value of k was estimated based on the time to remove one monolayer of reaction product at 35°C for 50% duty cycle given the PER and InP unit cell height. The values of α and I were extracted from the fitted curves in Fig. 3.7. The model predicts the PER behaviour for frequencies of 15 Hz and 100 to 3200 Hz at 35°C for duty cycles between 10 and 100%. Both the experimental and calculated values show that the PER is relatively independent of frequency between 100 and 3200 Hz. For a frequency of 15 Hz, the approximation kt_{off}<<1 can not be made. Consequently, a frequency dependence is expected and both the experimental and calculated values of Fig. 3.7 show this dependence. PER versus irradiance was calculated at 20, 35, and 45°C using k=55, 140, and 255 respectively. Calculated R_{ph} versus 22I is presented as solid lines superimposed on the experimental data in Fig. 3.5. The

mathematical factor 22 is introduced so that I used in Eq. (3.3) could take on a physical meaning of irradiance with units of W/cm^2. The curves represent a good fit with the correct saturation behaviour. An Arrhenius treatment of the k values predicts an activation energy of 0.50±0.05 eV. This value is much larger than that obtained from PER versus temperature studies. An explanation for this discrepancy is that at the low temperatures the etching process proceeds at the irradiance saturation level, however, this is not the case for the high temperature data since the irradiance saturation level is temperature dependent. If the data were obtained at an irradiance level which was greater than or equal to the high temperature saturation level, then R_{ph} would be larger than reported at high temperatures and unchanged at low temperatures. This would correspond to an activation energy larger than the 0.34±0.03 eV that was observed from the PER versus temperature studies.

3.4 Summary

Photochemical etching behaviour of n-InP was studied as a function of sample thickness, electrolyte temperature, and pH, laser irradiance, and illumination duty cycle and frequency. By optimizing these variables, the PER was

enhanced by an order of magnitude to over 13 μm/min. The etching process was shown to be reaction rate controlled with a thermal activation energy $\geq 0.34 \pm 0.03$ eV. The effects of illumination duty cycle and frequency on PER were accounted for based on a rate equation model for the removal of reaction products from the semiconductor surface. Although the data was obtained by producing vias, under the present experimental conditions it is applicable to other modes of surface modification of n-InP such as grooves and gratings.

Chapter 4. The Influence of Metal Ion Impurities on Photoetch Rate

4.1 Introduction

The data presented in Chapter 3 were obtained using a single line Ar^+ laser at 488 nm and 4.3 mW while keeping the electrolyte height constant. The data presented in this chapter were obtained using a multiline (predominantly 488 and 514.5 nm) Ar^+ laser at 10.0 mW. Upon changing the laser, the apparatus used to maintain a constant fluid height was disconnected. With etching at room temperature the effect of fluid evaporation on focal length was found to be negligible. However, the resulting PER at room temperature with a 50% duty cycle at 200 Hz was significantly lower than that reported in Chapter 3.

The PER data obtained using a higher irradiance (the $1/e^2$ spot size of both lasers was 600 μm) was expected to be equal to or slightly greater than that obtained using a lower irradiance level. This assumption was based on the predicted and observed saturation behaviour presented in Fig. 3.5. The explanation for this unexpected result was investigated by a series of simple experiments. The tests proved that when

copper was dissolved in the electrolyte the PER increased. The source of the copper ions was the two copper probes used to keep the fluid height constant as copper is soluble in phosphoric acid with a pH of 2.0 [33].

This chapter discusses a possible mechanism of metal ion impurity enhanced photoetching. A reaction sequence is proposed and experimental evidence supporting the proposal is presented.

4.2 Reaction Sequence for Enhanced Photoetching

Photoetching in an open circuit situation requires that the cathodic current equal the anodic current and that the redox reactions take place at the same potential, the open circuit potential [12,16]. The cathodic reaction occurring in this electrolyte at the dark regions without metal ions in solution using photo generated electrons is most probably the reduction of dissolved oxygen [16]. With metal ions in solution there may now be a competing reaction involving reduction of metal ions at the semiconductor surface,

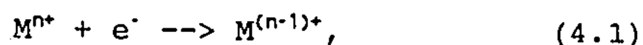

$$M^{n+} + e^- \rightarrow M^{(n-1)+}, \qquad (4.1)$$

where n is an integer representing the oxidation state of the metal M.

The concept of adding impurities to electrolytes in an

effort to improve the photo cathodic performance has been reported in solar cell work [34]. Also, Gerischer, Pettinger, and Lubke [35] have reported on electrochemical reactions on semiconductor surfaces catalysed by submonolayers of deposited metal atoms. The presence of platinum and gold increased both cathodic and anodic current densities by greater than two orders of magnitude depending upon the amount of metal coverage. Adsorbed dye molecules with cobalt and copper as central atoms were also reported to catalyse various reactions resulting in higher current densities on semiconductor surfaces. The catalytic activity was attributed to the d-band character of the metals. This explanation is often quoted as an explanation for the catalytic behaviour of metals [36].

In order for the proposed reaction in Eq. (4.1) to be a possible explanation for the enhanced PER of n-InP, the redox potential must lie in a potential range which overlaps with the anodic oxidation potential of InP. The anodic oxidation potential of InP (Eq. 1.1) lies at approximately 0 V with respect to the Saturated Calomel Electrode (SCE) [37,24]. The standard redox potential for oxygen reduction is ≈160 mV (SCE), and for copper ion reduction it is ≈100 mV (SCE) [38]. Thus, it is possible that with copper ions in solution another electron transfer process involving the reduction of copper ions can take place as opposed to the

oxygen reduction reaction.

The structure of the metal-semiconductor interface is unknown. However, it is proposed that while light is on the semiconductor, electron transfer to copper ions near the semiconductor surface takes place resulting in adsorbed Cu and/or Cu^+. Shortly after the light is turned off the adsorbed copper re-solvates returning to the electrolyte in a non-copper consuming process. The possibility that Cu^{2+} injects a hole into the valence band which then recombines with an electron resulting in an enhanced PER is not highly probable since the copper redox level is estimated to be about 500 mV (SCE) negative with respect to the valence band edge [37].

Laser assisted deposition of both metals and semiconductors onto various substrates has been demonstrated [39]. The technique, known as laser direct writing, usually involves UV light and the species to be deposited is in a complexed form, usually an organometallic. The mechanism is either pyrolytic or photolytic. Pyrolytic deposition involves laser heating of the substrate and results in bonding between adsorbed species and the substrate due to the elevated substrate temperature. Photolytic deposition involves the breakdown of the organometallic complex due to photon absorption allowing an electronic interaction between the substrate and the newly created radical. These mechanisms

are different from the electronic process proposed in this chapter.

4.3 Metal Ion Impurity Enhanced Photoetch Rate

The concentration of copper in solution was 4.1±0.5 ppm or 2×10^{-4} molar as determined by neutron activation analysis. Other metals both soluble and insoluble in phosphoric acid were tested for their ability to enhance the PER. Both magnesium and zinc are soluble, yet both metals did not enhance the PER when dissolved into solution. The redox potentials of magnesium and zinc are, respectively, approximately 2.6 and 1.0 V less than that for anodic dissolution of InP. Therefore, enhanced photoetching is not expected with these metal ions as there is no overlapping potential range for the anodic and cathodic reactions to proceed simultaneously.

Gold is insoluble in this electrolyte and as expected when a gold wire was inserted into the electrolyte there were no signs of enhanced photoetching. However, when a gold wire bond was made to the sample surface with an ultrasonic wire bonder the PER (without copper ions in solution) was enhanced. Noble metals in electrical contact with semiconductor surfaces have been reported to act as cathodes for the reduction

reaction on illuminated samples [17]. However, this does not account for the enhanced PER observed. As discussed earlier, gold is an effective agent for increasing the exchange currents on semiconductor electrodes [35]. It is believed that the gold wire acts as sink for the photogenerated electrons and the cathodic half reaction proceeds on the gold wire at a much faster rate. Since the anodic and cathodic partial currents must be equal, increasing the cathodic current also increases the anodic current given that the anodic current is not limiting. This results in a higher PER.

In an effort to increase the PER over 1.2 μm/min, four gold wire bonds were made to the sample surface. The PER, however, did not increase above 1.2 μm/min. This was also the case for electrolytes with higher concentrations of copper. Also, although the power levels used in this study were 2.5 times greater than that used in a Chapter 3, the PER did not significantly increase. This is consistent with the PER model which predicted a saturation of PER for irradiance levels near 200 W/cm^2 for a 50% duty cycle at room temperature (Fig. 3.5). It is therefore believed that this rate represents an upper bound for these experimental conditions.

The surfaces of photoetched samples were examined in a scanning Auger microscope for the presence of copper at non-illuminated regions. No copper was detected on the n-InP. This is consistent with the physical model of copper ion

reduction during illumination and solvation during non-illuminated periods. At some value of electron transfer rate, the amount of copper deposited onto the semiconductor surface will become greater than that going back into solution. The result being copper plating on the non-illuminated regions of an n-type semiconductor.

It is well known that the PER for GaAs is significantly greater than that for InP [9], consequently, the rate of electron transfer is significantly greater. A piece of n-GaAs was photoetched under the same conditions used in etching n-InP. As with InP, it is thermodynamically possible for the reaction presented in Eq. (4.2) (with copper as the metal) to be carried out on GaAs [37]. After photoetching, the non-illuminated regions of the n-GaAs appeared to the naked eye to be covered with a copper coloured film. The presence of copper on the sample was confirmed by Auger electron analysis as shown in Fig. 4.1. The characteristic copper peaks are marked along with the usual contaminants of carbon and oxygen. Sulphur was another contaminant detected along with phosphorous leftover from the electrolyte. Possible sources of sulphur contamination are from handling the specimen after etching before placing it into the vacuum system, and possibly accumulation of the n-type dopant on the surface after etching.

Another more significant test of the theory was to try to

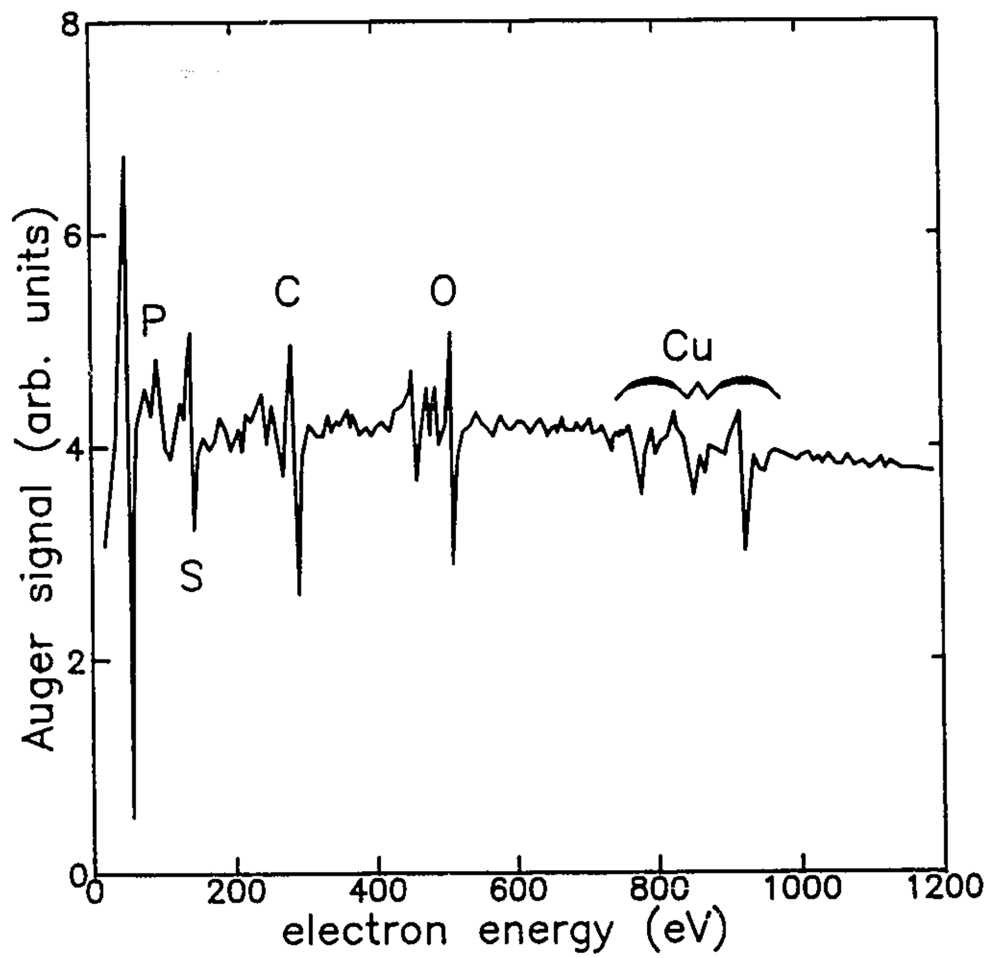

Fig. 4.1 Auger electron spectra from the dark regions of photoetched GaAs confirming the presence of copper.

deposit copper onto p-type InP. As discussed earlier, due to band bending, when a semiconductor is non-uniformly illuminated minority carriers are confined to illuminated regions while majority carriers travel away from the illuminated regions. Thus, in p-type semiconductors the electrons are confined underneath the light source. For similar electron and hole generation efficiencies, the reduced cathode area results in a cathodic current density increase of 2-3 orders of magnitude over n-type semiconductors for these experimental conditions.

For approximately 10 hours p-InP was continuously illuminated while immersed in a copper charged phosphoric acid electrolyte. The light source was that from the multiline argon ion laser at 10.0 mW unfocused. As shown in Figs. 4.2a and 4.2b, copper was deposited onto the sample. The region of deposition was confined to the illuminated region. The bright central region (labelled 3), corresponding to the deposited copper, was surrounded by a region which did not have copper deposited on it (labelled 2); this region was not noticeably etched. The region outside the two concentric circles (labelled 1) was etched as shown in the alpha-step profile, Fig. 4.3. Etching of the non-illuminated regions was not uniform, the most severe etching occurred at the anode/cathode boundary.

The existence of the two concentric rings in Fig. 4.2a is

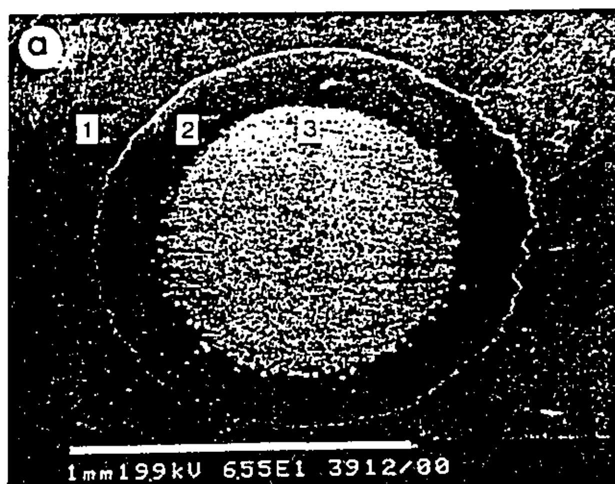

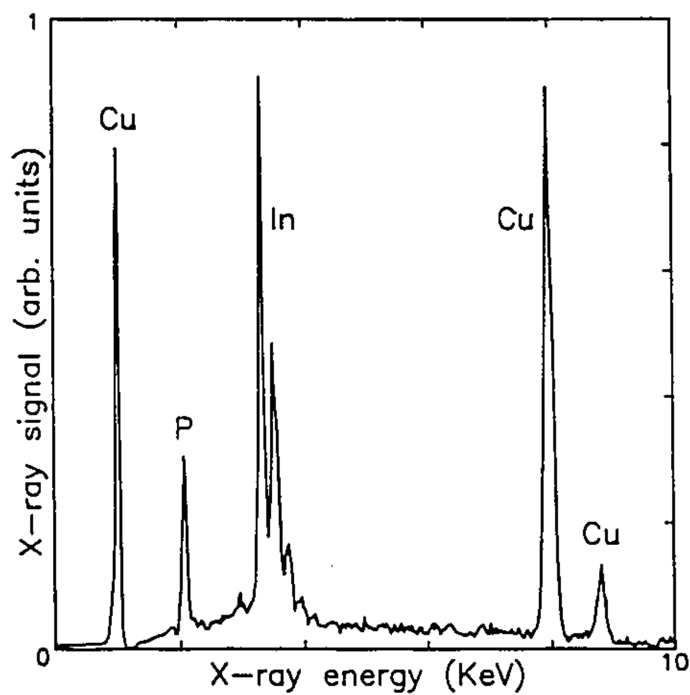

Fig. 4.2 Copper deposit on p-InP. a) Secondary electron micrograph of region directly under the incident Ar^+ laser beam. b) Confirmation of copper deposition by EDAX.

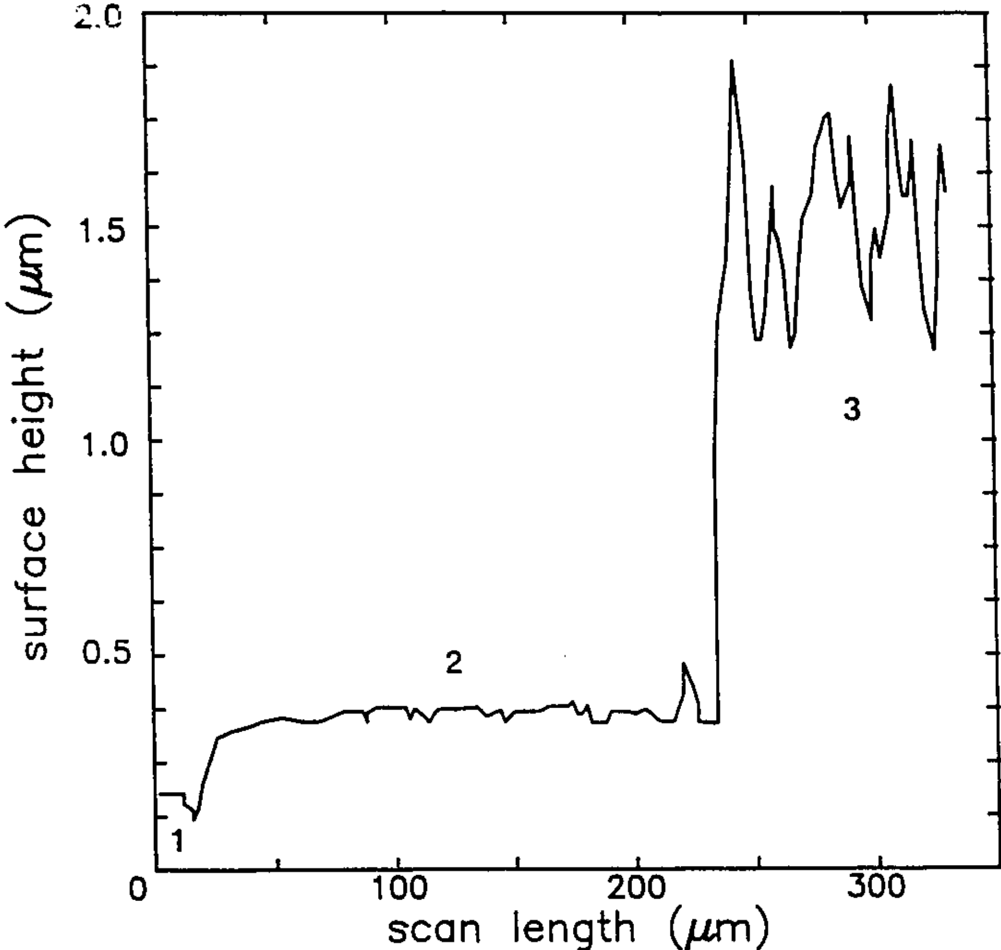

Fig. 4.3 Mechanical stylus profile of p-InP illuminated by Ar^+ laser beam shown in Fig. 4.2.

understood when the intensity profile of the unfocused laser is considered. The beam intensity profile was measured and is presented in Fig. 4.4. The diameter of the laser beam (where the intensity falls to ≈1% of the maximum value) was the same as the diameter of the large ring, ≈1280 μm. The area defined by the laser beam acted as the cathode, and at sufficient irradiance (therefore current density) copper was plated onto the p-InP substrate. The average thickness of the copper was ≈1.75 μm. It is important to note that when two spots were illuminated one after each other for 4 hours each, the copper deposited under the first spot went back into solution as the second spot was being illuminated. This indicates that the deposited copper is not resistant to the electrolyte.

4.4 Summary

The redox reactions and reaction mechanisms reported in this chapter have not been directly measured and confirmed by electrochemical techniques. However, the experimental evidence and the literature seem to confirm that the proposed reaction sequence of metal ion impurity enhanced photoetching is possible. The absence of copper on the non-illuminated regions of n-InP is consistent with the physical picture. This is also not surprising considering the high current

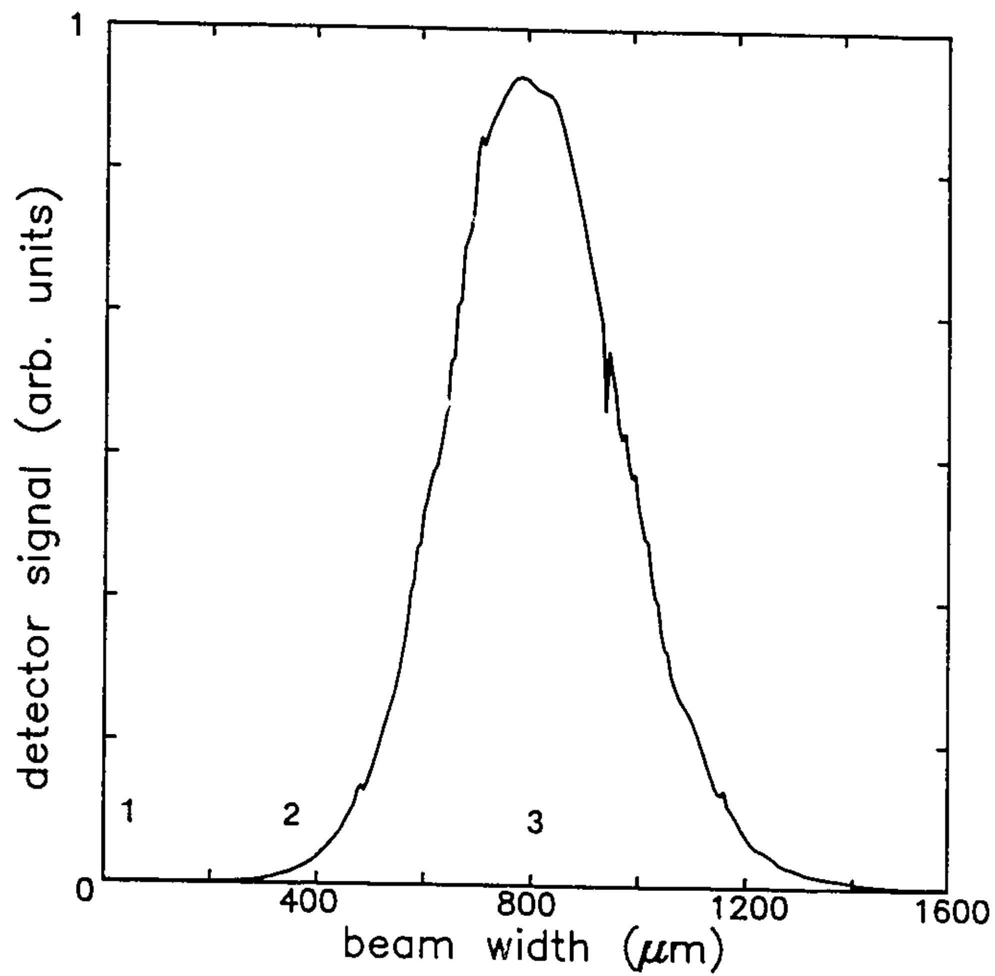

Fig. 4.4 Measured intensity profile of incident Ar^+ laser beam.

density necessary to deposit copper on p-InP, and that the deposited copper was not permanent.

For samples with gold wire bonds to the surface, the enhanced PER was attributed to the ability of gold to increase the cathodic reaction. In both cases, an alternative path for the reaction of photogenerated electrons with the electrolyte was provided which resulted in a significantly higher PER.

Chapter 5. Photoetch Rate as a Function of Surface Quality and Preparation

5.1 Introduction

This chapter reports on the photoetching behaviour of n-InP as a function of surface preparation. Sample preparation involved mechanical lapping the as received wafers in succession using 14.5 μm, 5.0 μm, 1.0 μm, 0.3 μm, and 0.05 μm alumina powders suspended in de-ionized water. The surfaces were characterized by cross sectional transmission electron microscopy, photoluminescence, scanning electron microscopy and mechanical stylus profiling. The PER of n-InP was found to increase as the surface roughness increased for no copper in solution.

Samples with a nominal surface area of approximately $1.0X0.8\ mm^2$ were cleaved from the polished wafers for the photoetching experiments. The frequency of chopped light was kept constant at 200 Hz with a 50% duty cycle. All experiments in this chapter were carried out at room temperature.

5.2 Photoetch Rate and Surface Preparation

Surface treatment prior to photoetching had a pronounced affect on the PER of samples when copper was not introduced into the electrolyte. As shown in Fig. 5.1, the PER increased with increasing polishing powder size for the 0.0-1.0 μm and 5.0-14.5 μm powders. For this work, chemical polishing with a Br:MeOH solution is considered to be polishing with a powder size of 0.0 μm.

The 1.0, 0.3, and 0.05 μm powders were white in colour while the 14.5 and 5.0 μm powders were grey. All powders were supplied by Buehler Limited. For each polishing step a new polishing cloth was used and polishing was performed for no less than 15 minutes at each stage. Chemical polishing with a solution of 1% bromine in methanol (Br:MeOH) by volume followed by a methanol quench was also carried out for some samples. The discontinuity between results obtained with the 0.0-1.0 μm and 5.0-14.5 μm polishing powders is thought to be due to the powder morphology. The 0.05, 0.3, and 1.0 μm powders were blocky shaped whereas the 5.0 and 14.5 μm powders were flaky [40]. The 5.0 and 14.5 μm powders produce a smoother (i.e., less damaged) surface than expected; the 5.0 μm powder was found to produce a smoother surface than the 1.0 μm powder. All the powders had the alpha or hexagonal structure with a hardness value of 9 on the Mohs scale except

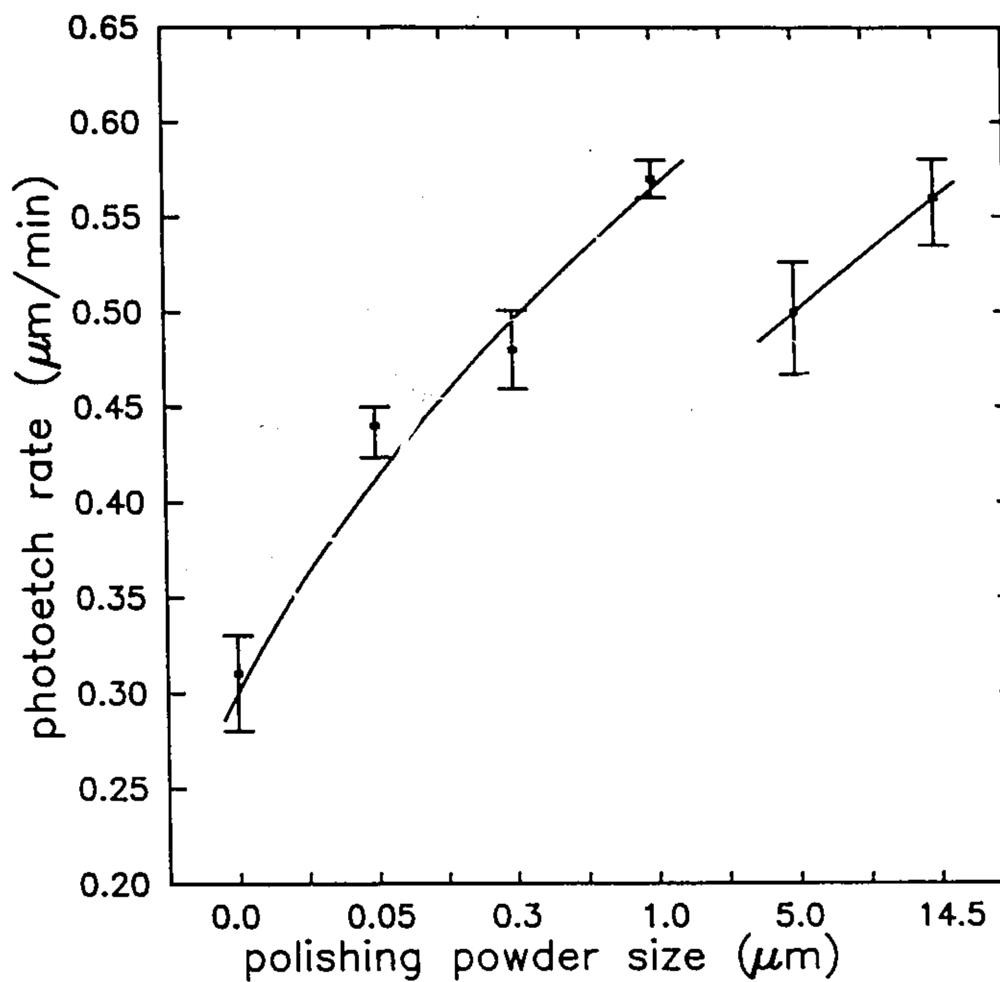

Fig. 5.1 Photoetch rate versus polishing powder size at 20°C, 200 Hz, and 50% duty cycle. Polishing with Br:MeOH is considered to be polishing with a powder size of 0.0 μm.

the 0.05 μm powder which had the gamma or cubic structure with a hardness of 8 on the Mohs scale.

The photoetching process requires the generation and separation of electron-hole pairs so that they may freely participate in the cathodic and anodic reactions respectively. It has been shown [39,41] that heavily damaged regions are insensitive to photoetching presumably due to free carrier recombination. It was therefore expected that higher quality surfaces would have higher PERs yet the opposite was observed experimentally.

After these initial results, a second set of samples were prepared by polishing in a similar manner as outlined above to test the validity of the unexpected results. The actual data differed slightly from the first data set in that the PER was on average 16% lower, however, the trends were the same.

5.3 Photoetch Rate and Surface Quality

The profile of polishing induced surface damage for the various surface treatments was determined by viewing specimens in cross section with a transmission electron microscope. The samples were prepared by dimple grinding followed by ion milling with argon gas at liquid nitrogen temperature as outlined in Chapter 2. The samples were examined in a Philips

CM12 microscope at 120 kV. Surfaces prepared by polishing in Br:MeOH had relatively little surface damage; the damage extended approximately 6 nm into the bulk. All other surfaces had three distinct regions of differing dislocation density. There was a very heavily damaged region at the surface with the highest dislocation density. Underneath this layer was a thicker damaged region with a lower dislocation density followed by a third region containing isolated dislocations propagating into the bulk. Micrographs of the Br:MeOH and 14.5 μm polished samples are shown in Fig. 5.2. The variation of dislocation depth with polishing powder size for all three regions is shown in Fig. 5.3. In comparing Fig. 5.1 and Fig. 5.3, a similar two regime behaviour is evident. Dislocation depth increased with polishing powder size up to 1.0 μm then markedly decreased at 5.0 μm consistent with the PER versus polishing powder size data. It is important to note that the absorption depth of 514 and 488 nm light in InP is approximately 90 and 73 nm respectively [42]. Thus for all samples, excluding the Br:MeOH treated ones, the light is absorbed within the damaged regions.

Semiconductor surface quality is often characterised by photoluminescence (PL). For a given semiconductor the peak PL intensity is higher for high quality surfaces than for surfaces with high defect densities [43]. In damaged surfaces, generated carriers have a higher probability for

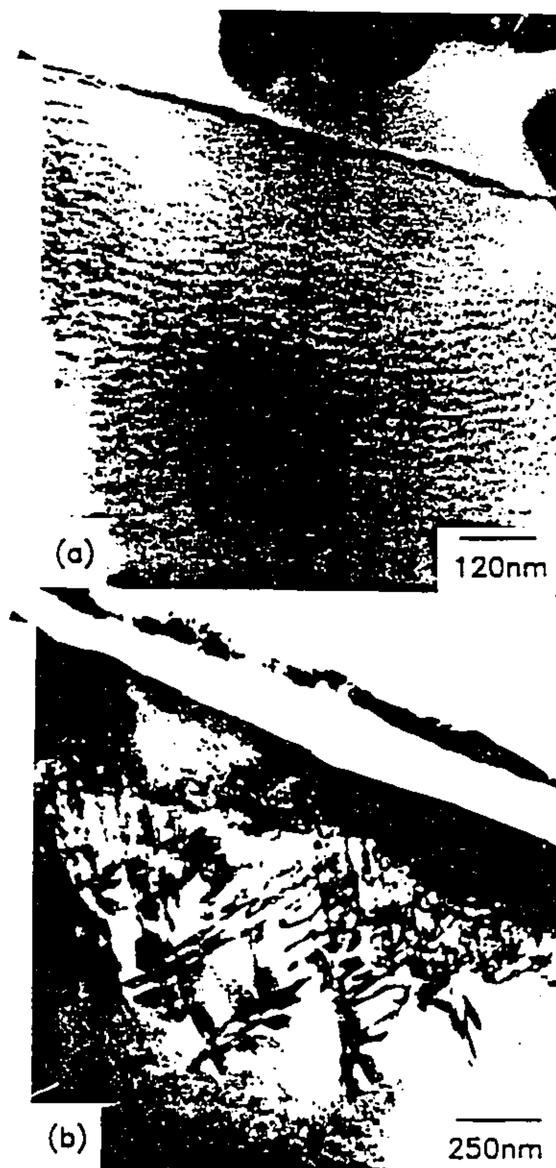

Fig. 5.2 Cross sectional bright field transmission electron micrographs of samples with surfaces prepared using a) Br:MeOH and b) 14.5 μm alumina powder. The arrows indicate the sample surface. Silvar epoxy is seen as dark regions at the top right hand side of the micrographs.

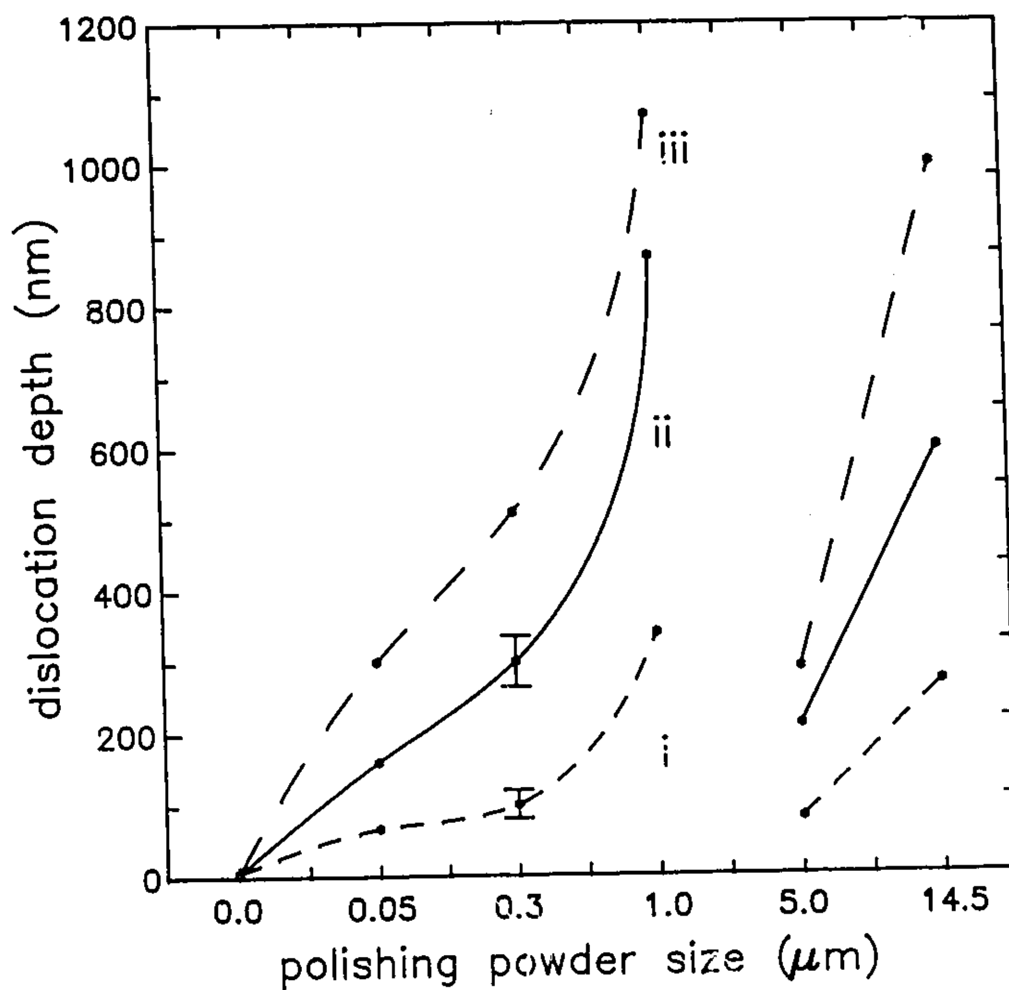

Fig. 5.3 Dislocation depth from the free surface as a function of polishing powder size for three regimes of dislocation density i) heavy ii) moderate and iii) low dislocation density.

non-radiative recombination with a shorter lifetime and decreased di..fusion length. The peak PL intensity (corresponding to ≈860 nm) was measured at 14 Kelvin using an argon ion laser at 488 nm and 2.4 mW. The results were consistent with the dislocation depth data and inversely proportional to the PER as shown in Fig. 5.4. The highest PL yield corresponded to the lowest PER (bromine-methanol) and the lowest PL yield corresponded to the highest PER (14.5 μm). Also, the samples polished with 5.0 μm powder showed an increase in PL yield and a decrease in PER compared to the samples prepared with 1.0 μm powder as shown in Fig. 5.1 and Fig. 5.4.

Fig. 5.5 shows two vias photoetched under the same conditions for samples polished using Br:MeOH and 14.5 μm powder. The width of the via etched on the sample polished with Br:MeOH was significantly larger than the sample prepared using the 14.5 μm powder. Also, the surface around the via was lightly etched indicating longer diffusion lengths. These observations are consistent with the PL data.

5.4 Photoetch Rate and Surface Roughness

Surface roughness was evaluated both qualitatively using a scanning electron microscope and quantitatively using a

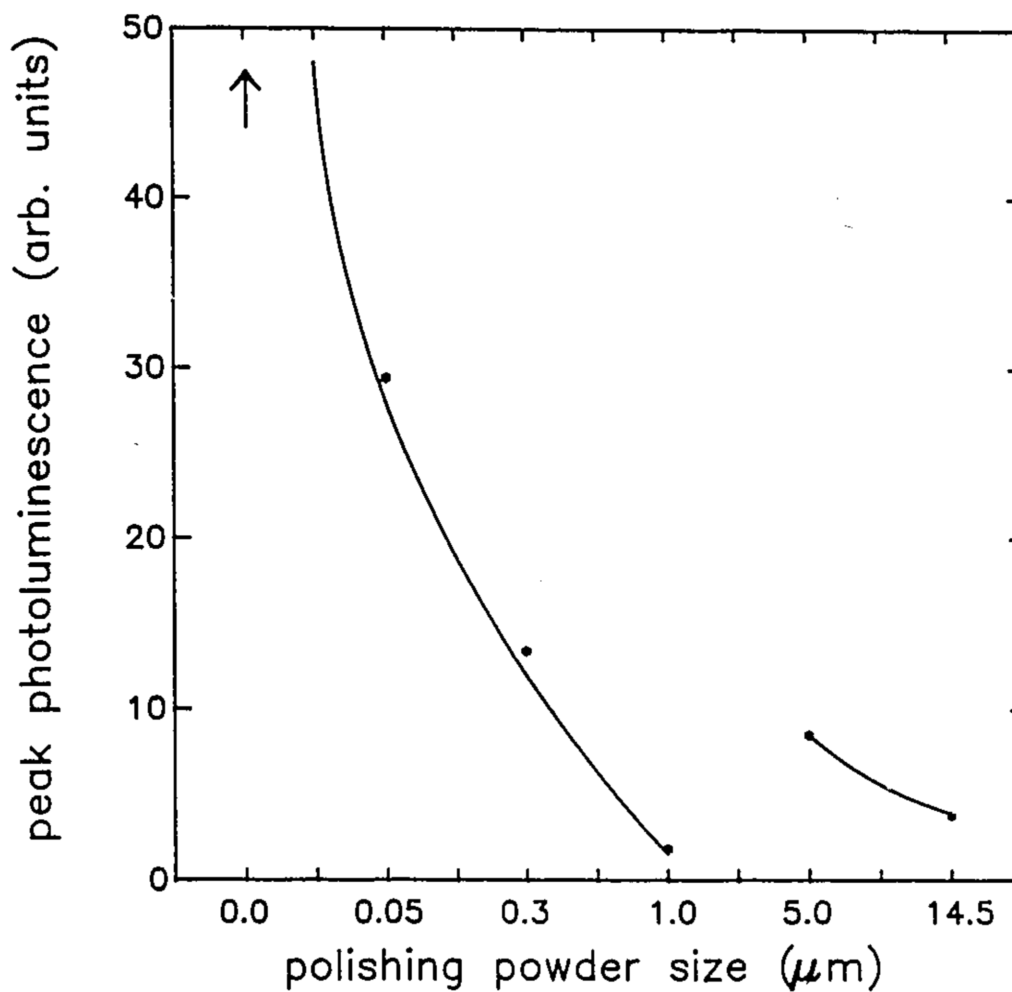

Fig. 5.4 Peak photoluminescence (PL) intensity versus polishing powder size at 14 Kelvin using 488 nm light at 2.4 mW. The peak PL signal from the Br:MeOH sample was 132 a.u. as indicated by the arrow.

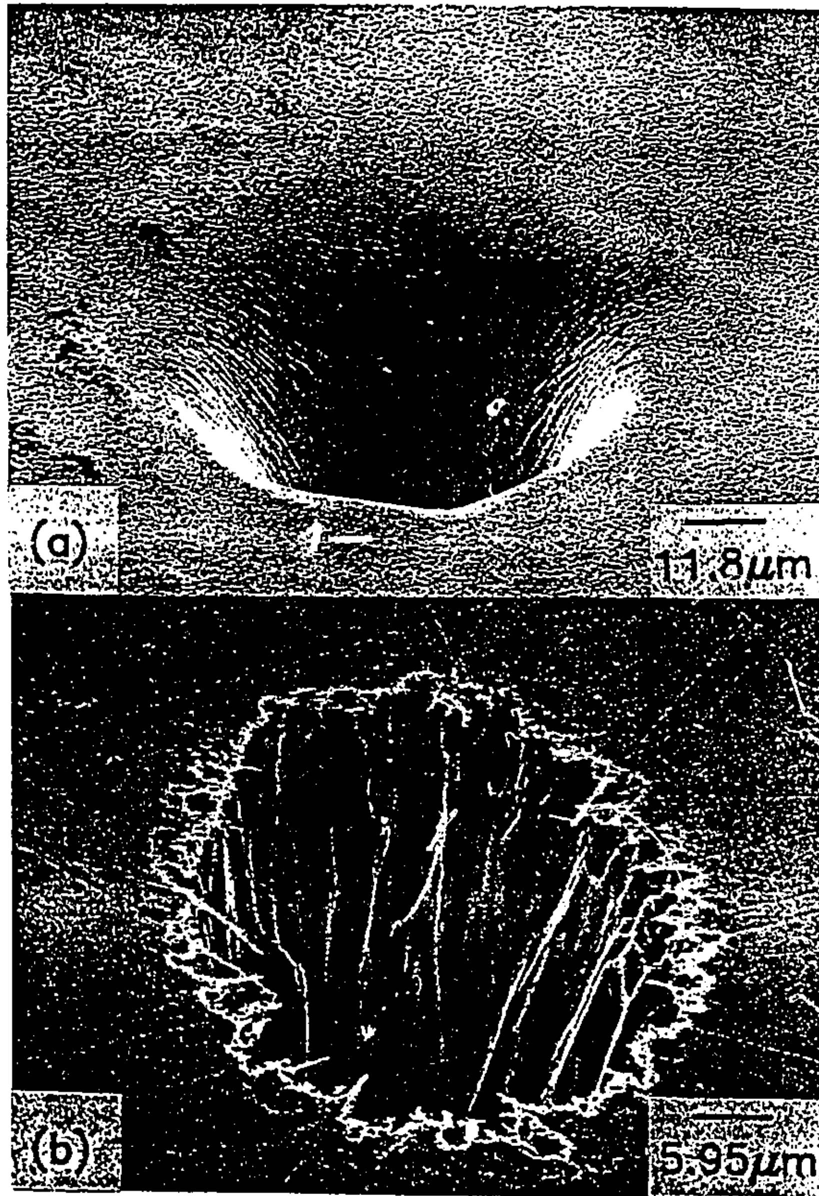

Fig. 5.5 Top view of two vias etched under identical conditions for surfaces prepared with a) Br:MeOH and b) 14.5 μm alumina powder.

Tencor alpha-step with a 12.5 μm diamond tipped stylus. As can be seen in Fig. 5.6(a-f), surface roughness appears to increase progressively with powder size with the exception of the sample polished with 5.0 μm powder.

For a quantitative measure of surface roughness the x-y scan from the alpha-step was digitized and converted to total distance travelled as the stylus moved up and down while it traversed the sample. This distance was then normalized by dividing through by the scan length and then squared to give an effective surface area factor. Using Fig. 5.7, the effective surface area factor, F, is given in Eq. (5.1) as,

$$F= (\Sigma((x_i-x_{i-1})^2+(y_i-y_{i-1})^2)^{1/2}/(x_n-x_0))^2, \qquad (5.1)$$

where n is the number of points in the summation and (x_n-x_0) is the scan length. The effective surface area is defined as surface area multiplied by the effective surface area factor for each surface treatment.

The effective surface area factors are given in Table 5.1. The factors increased with polishing powder size up to 1.0 μm and showed the familiar discontinuity or two regime behaviour for the 5.0 and 14.5 μm powder. This indicates that polishing powder size is not a measure of surface roughness. The effective surface area factors are expected to be underestimated because of the measuring process

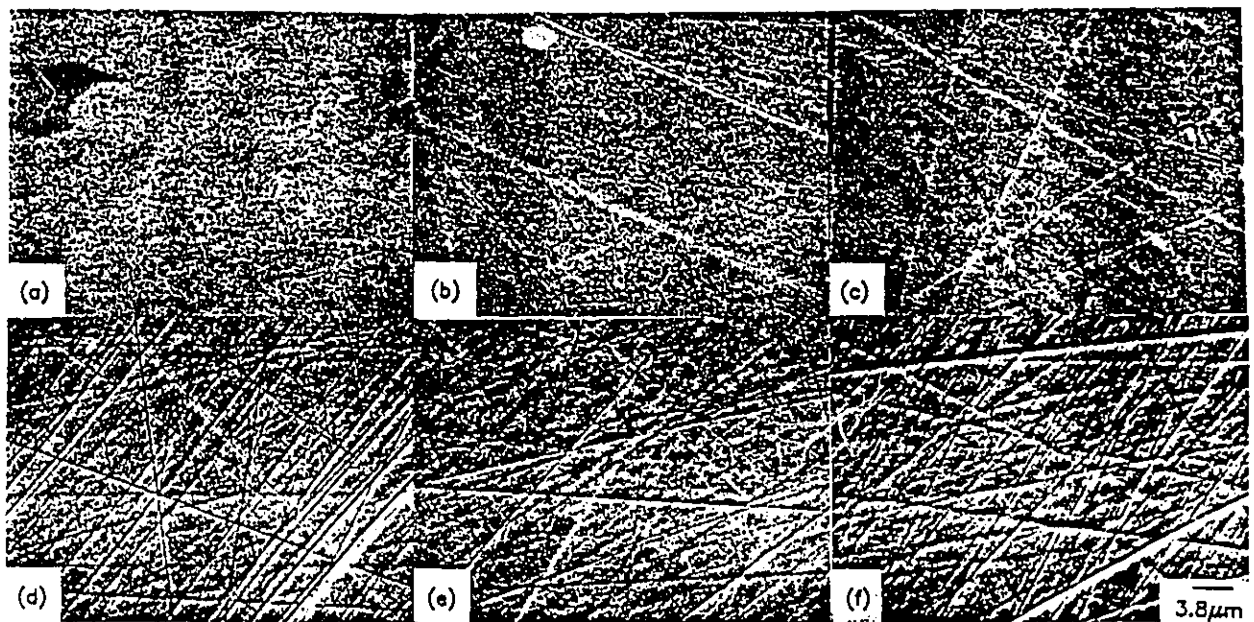

Fig. 5.6 SEM secondary electron images showing surface roughness with polishing powder size. All samples were etched with HF:HBr 5:1 by volume for 30 s at room temperature. a) Br:MeOH b) 0.05 c) 0.3 d) 1.0 e) 5.0 and f) 14.5 μm alumina powder.

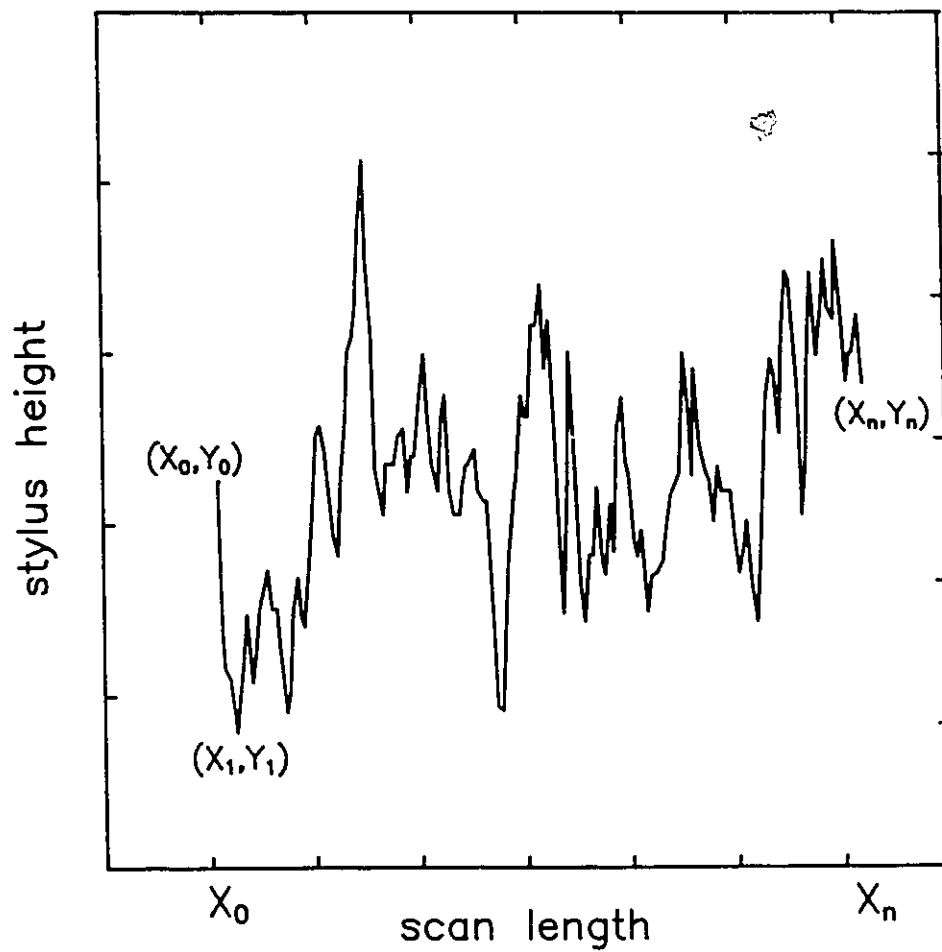

Fig. 5.7 An example of a mechanical stylus profile illustrating how the effective surface area factor (F) was calculated.

Table 5.1 Effective surface area factor (F) with surface preparation.

Sample	Br:MeOH	0.05μm	0.3μm	1.0μm	5.0μm	14.5μm
F	2.0	2.2	3.0	5.0	3.6	6.2

as the stylus is incapable of precisely reproducing surfaces especially those with sharp or deep features.

For a given sample the effective surface area may be changed either by increasing its physical size or by changing the surface pretreatment. The effect of changing the physical size of the samples on PER was investigated. The variation of PER with effective surface area for samples polished with 0.05 and 14.5 μm powders is given in Table 5.2. The data clearly show that PER increased with increasing surface area for a given surface treatment (this is also true for other polishing powder sizes not shown). Also samples with different surface treatment and equivalent effective surface area had similar PERs. Also, smoother surfaces tended to have slightly higher PERs than rougher surfaces with equivalent effective surface areas. This result may be real, or it may be due to the inaccuracy of the effective surface area factors or experimental scatter. Until a truly accurate effective surface area factor can be obtained, and obtained for each sample, it will be difficult to access this observation. This is consistent with work on GaAs that showed an increasing etch rate with sample surface area in electrolytes where the reduction reaction on the surface was limiting [16].

More importantly, however, the data explains the behaviour of PER with polishing powder size. Samples prepared with 0.05 μm polishing powders could have PERs greater than

Table 5.2 Effective surface area and photoetch rate for samples prepared with 0.05 and 14.5 μm powders.

	0.05μm				14.5μm			
Effective surface area ($10^5 \mu m^2$)	7.2	26.2	58.8	345.1	8.9	22.0	62.8	632.4
Photoetch rate (μm/min)	0.29	0.39	0.47	0.81	0.24	0.36	0.44	0.84

those polished with 14.5 μm powders by changing their relative surface areas (i.e., the size of the sample). Conversely, it is possible that a physically small sample prepared with 14.5 μm polishing powder could have a higher PER than a larger sample prepared with 0.05 μm powder. These observations are significant. The data indicate that the effective surface area dictates the PER and not simply the physical size and also that PER is independent of surface quality as characterized by dislocation depth and peak PL for these mechanically polished samples. The larger surface area means a larger non-illuminated region is available for the cathodic reaction involving photogenerated electrons.

5.5 Summary

Photochemical etching behaviour of n-InP was studied as a function of surface preparation. The surfaces were prepared by chemical and mechanical polishing with Br-MeOH and alumina powders respectively. Surface characteristics evaluated using cross sectional transmission electron microscopy, photoluminescence, scanning electron microscopy, and mechanical stylus profiling were dependent upon both the polishing powder size and morphology. The variation of PER with surface preparation was shown to be due to the difference

in effective surface area. Coarser polishing powders produced rougher surfaces resulting in larger effective surface areas. Samples prepared with the 0.05 μm powder needed three times the surface area of samples prepared with the 14.5 μm powder to have a comparable PER. Also, for samples with copper ions in solution or gold wire bonds, the PER saturated at ≈1.2 μm/min and was strongly not dependent upon surface preparation.

For samples etched with copper ions in solution or with gold wire bonds, the PER was limited by the removal of reaction products as shown in chapter 3. For samples without copper or wire bonds the PER was limited by the rate of the reduction reaction on the surface involving photo generated electrons. The two situations represent two different kinetic regimes.

Chapter 6. On the Question of Local or Global Saturation

6.1 Introduction

Saturation of PER was demonstrated in Chapter 3 as a function of irradiance and temperature, and again in Chapter 5 as a function of electrolyte metal ion impurities and surface gold wire bonds. The work reported in this chapter was undertaken to determine if the saturation behaviour was locally or globally controlled. The saturation behaviour is said to be under local control if the rate of material removal is controlled by local conditions and not what processing may be happening simultaneously or previously at another site on the sample surface. Conversely, saturation is said to be under global control if local rates of material removal are affected by additional remote surface processing.

Studies on n-InP indicated that the photoetching process was globally controlled [18]. It was reported that the rate of material removal from n-InP was controlled by an additional secondary light source. The light source simultaneously illuminated the sample as the primary light source etched the surface. The light source was a low irradiance large area beam (10 mW/cm^2, and 2 mm in diameter). The irradiance of the

secondary light source controlled the etch rate that was obtained with the primary light source. The etch rate decreased as the irradiance of the secondary light source increased. However, the illuminating wavelength did not affect the amount of etch rate reduction for a given irradiance level.

6.2 Experimental

A set of experiments were designed to test for local or global saturation of the photoetching process. The experiments involved illuminating the sample surface with two spots of light with equal intensity. Any significant difference in PER between etching with one beam and two beams would indicate that the process was globally saturated, while no significant difference would indicate local saturation.

Illumination with two beams using one light source was accomplished by using a beam splitter. The intensity in the two beams was measured to be the same to within 4%. The two beams were then directed onto the sample surface through an objective lens as outlined in Chapter 2. As already indicated, the purpose of the experiments was to measure the PER when only one via was produced, and then when two vias were produced simultaneously. This was accomplished by incorporating a computer controlled beam blocker into the

experimental apparatus. This enabled the production of one or two vias at a time by simply blocking or not blocking one of the two incident beams. In the experiments, tests with one and two vias were etched alternatively. That is, odd numbered tests were performed with one spot of light, and even numbered tests were performed with two spots of light. Each experiment had a total of 10 tests. Alternating the tests in this way was done to eliminate any systematic error or bias introduced by performing tests of one type followed by tests of the other.

In another experiment a mechanical chopper was positioned in such a way that, for the first part of the chopping cycle, beam one was blocked while beam two was etching, and for the second part of the chopping cycle, beam two was blocked while beam one was etching. Once again, using the beam blocker, even numbered tests had two illumination sources and odd numbered tests had only one illumination source. For tests with two illumination sources, the experimental situation was equivalent to instantaneously moving one beam from via one to via two. For these experiments the sample was continuously illuminated, however, each of the two vias were etched with a 50% duty cycle. The purpose of this experiment was to test for local or global saturation. By comparing the PER obtained while producing two vias with the PER of one via all at 50% duty cycle, local or global saturation could be determined.

No significant difference in PER would indicate local saturation while a significant difference would indicate global saturation.

In all experiments the fluid height was maintained at a constant level using inert platinum wires in place of the copper probes outlined in Chapter 2. This enabled experiments to be performed on samples with and without metal ion impurities simply by inserting or not inserting a copper wire in the electrolyte prior to and during the experiment. The distance between the two vias etched simultaneously varied from 240-650 μm. A mechanical chopper at 200 Hz was used in experiments where the duty cycle was not 100%. The samples were prepared by polishing with 14.5 μm alumina, and the experiments were performed at room temperature.

6.3 Evidence for Local Saturation of Photoetch Rate

The investigations represent a wide range of experimental conditions including different irradiance levels, sample size, duty cycle, electrolyte impurity levels, and distance between the two sources of illumination. The data for the experiments are shown in Table 6.1. As mentioned in the earlier sections of this chapter, global saturation would manifest itself as a significant difference in PER for samples with one and two

Table 6.1 Average difference in measured PER between vias produced with one illuminating spot and two illuminating spots on the sample surface. The difference is expressed as a percentage and in all cases the difference is within the experimental scatter of the data.

Experimental conditions	PER with one via	PER with two vias	% change in PER
100% duty cycle, Cu present light sources 240 μm apart	1.07±.02	1.08±.03	0.9
5% duty cycle, Cu present light sources 630 μm apart	7.8±.6	7.6±.6	3.5
100% duty cycle, no Cu light sources 300 μm apart	0.80±.09	0.80±.10	0.0
5% duty cycle, no Cu light sources 630 μm apart	6.2±.24	6.16±.08	0.8
50% duty cycle, Cu present, two vias etched by effective movement of the etching beam light sources 240 μm apart	2.0±.1	1.9±.06	2.6

illuminated spots. In all cases the data obtained indicated that the PER was not significantly affected by the presence of an additional etching light source, as the average percentage difference in PER fell within the experimental scatter. Although the difference in PER fell within the experimental scatter, the PER for the tests involving two vias were less than the PER for one via 72% of the time. This indicated that there may have been a slight difference in PER with a secondary illumination source, however, the difference was not large enough to be statistically significant.

The results of the experiment designed to move the light source from via to via was significant. The data confirm that the photoetching process was locally saturated. It also indicated that the requirement for continued etching was that the light be removed from the area that was being etched and not that the light be totally removed from the sample surface. Thus, in order for the etching process to be most efficient, time must be provided for the reaction products to be removed from the reaction surface by the etching environment. If the reaction products have been allowed sufficient time to be removed, the effectiveness of the light energy will be increased due to the increased surface area available for further reactions. This picture is consistent with the results of section 3.2 which reported that the process was reaction rate limited.

The main implications of this work lie in the area of processing. The fact that it was possible to etch more than one via without reducing the PER is important for wafer production. Large scale processing of wafers requiring hundreds of vias would not be practical if simultaneous via production were not possible. Although the number of vias that could be etched simultaneously was not determined, the potential for large scale processing exists. The experiment involving movement of the light source indicates a potential for surface sculpting. As shown in Chapter 8, the illumination time required to produce the necessary reaction products for etching is on the order of 1 μs or less. Therefore, the light beam could be rapidly moved over the semiconductor surface in such a way as to produce varying depths of surface relief. The depth of etching would depend upon the number of times the light was incident at a certain point for a given beam scan rate. Beam movement could also be exploited for the application of thinning semiconductors for examination in the TEM. The beam could be moved around the sample surface in such a way that a dish, similar to that produced with dimple grinding, is produced. This would be an effective way to increase the thin areas in the photochemically thinned samples.

6.4 Summary

The question of local or global saturation of the PER was addressed. The photoetching process was found to be locally saturated by illuminating the sample with two beams simultaneously and comparing the PER with that obtained using only one beam. The results contrast with earlier work of Willner et al [18], however, the experimental conditions of the two pieces of work are different. The size and irradiance of the secondary light source along with a different electrolyte could account for the differences in the experimental findings. The fact that, for these experimental conditions, the photoetching process is locally saturated has some interesting processing implications for this work specifically, and semiconductor processing in general.

Chapter 7. Photoetching for Transmission Electron Microscopy

7.1 Introduction

Plan view samples for examination in the TEM were prepared by photoetching, ion milling, and chemical thinning. For semiconductors, ion milling is the most popular sample preparation technique, however, chemical thinning is becoming more widely used as it is a straight forward and quick technique to use. Photochemical etching is also quick, and for some specific applications it may be an extremely valuable method of sample preparation.

In the remainder of this chapter, photochemical etching as a method of sample preparation is evaluated by comparing various aspects of the three techniques outlined above.

7.2 Sample Evaluation

The bottom of via holes produced by photochemical etching were examined microscopically. As in other specimen preparation techniques, regions immediately adjacent to the perforation are generally transparent to the electron beam and

are imaged directly. One important advantage of this method of sample preparation is that the unthinned bulk material around the via acts as a self supporting ring stabilizing the fragile thin region and improving handleability. Artifacts such as cracks with associated dislocation networks were routinely observed in samples prepared by ion milling and chemical thinning but never in photoetched samples. This advantage also acts as a limitation. In electron microscopy it is essential that the specimen can be tilted through angles as large as ±25° in order to obtain both structural and chemical information. Thus, the geometry of the thinned sample places a limit on the sample thickness.

However, the most important feature of this new method is the ability to thin precisely predetermined regions with a built in stabilizing structure. Defect regions observed with other techniques such as luminescence, can be thinned and imaged directly thereby reducing the hit and miss approach in TEM sample preparation. These advantages become necessities when InP based lasers 250 μm by 300 μm in surface area are to be examined.

The main advantage of ion milling and chemical thinning is that the resulting transparent regions are orders of magnitude larger than that obtained by photochemical etching. Typical usable areas for photochemically prepared specimens are ≈75-200 μm^2. However, as mentioned above, large areas are

not necessary for examining small structures such as semiconductor lasers. Also, the results of Chapter 6 indicate that it may be possible to remove larger volumes of material resulting in a significant increase in the size of the electron transparent regions simply by rapidly moving the laser beam over the sample surface.

Ion milling InP presents a unique problem not associated with Si or GaAs. Due to the differential sputtering rates of In and P (P has a faster sputtering rate) the thinned regions are littered with In islands. The excess In easily migrates and coalesces on the sample surface due to beam induced heating. Two recommended solutions to the problem of contamination with In islands are to use a reactive species as the ion source, and to ion mill at liquid nitrogen temperature [44]. Additional processing of thinned samples is not recommended due to the extremely fragile nature of the thinned regions. In reactive ion etching, the reactive species (iodine was used in this work) reacts with the excess In thereby removing it from the specimen surface and eliminating the possibility of island formation. Ion milling at liquid nitrogen temperature decreases the mobility of any excess In so that it is sputtered away before it can migrate and coalesce into islands. Shown in Fig. 7.1a and b are micrographs of InP prepared by ion milling using iodine as the reactive ion source. The dark regions were positively

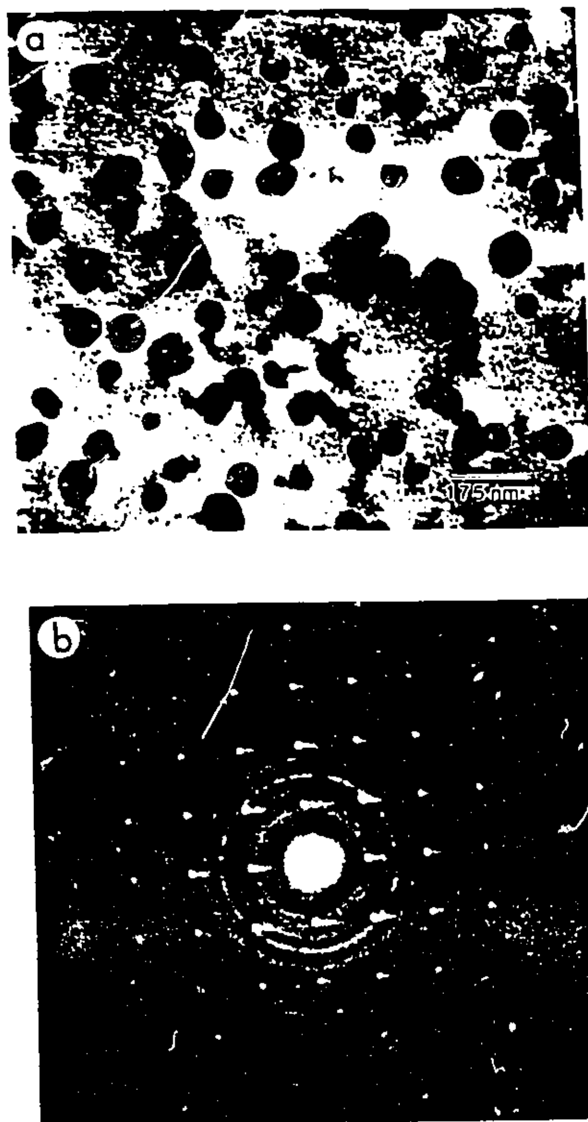

Fig. 7.1 TEM micrographs of single crystal InP prepared by reactive ion milling. a) Bright field micrograph showing dark regions corresponding to indium metal islands. b) Selected area electron diffraction pattern showing polycrystalline indium metal superimposed on the single crystal InP.

identified from the diffraction pattern as crystalline In. The underlying single crystal spot pattern is that of InP. Clearly the excess In has not reacted with the iodine. Similar results were obtained with argon gas as the ion source at room temperature. As shown in Fig. 7.2, when the sample was held at liquid nitrogen temperature the In islands were totally absent even with argon as the ion source. However, the InP did suffer significant radiation damage as seen in the micrograph and evidenced by a diffuse ring around the central spot in the diffraction pattern (not shown). Radiation damage is often a problem [45], however, it is possible to reduce the induced radiation damage by optimizing ion milling parameters such as accelerating voltage and specimen tilt.

Photochemically thinned samples also showed signs of preparation artifacts. At the hole periphery a thin extremely beam sensitive amorphous layer presumed to be an oxide left over from the photoetching process was usually present. The adjacent thinned material, however, does not seem to be compromised as shown in the micrographs of Fig. 7.3a, b, and c. There are some residual circular spots on the crystal, however, these regions disappear after short exposures to the electron beam and are concentrated near the amorphous layer. The thickness and composition of the amorphous oxide layer is the topic of section 7.3.

The single crystal samples examined in the microscope

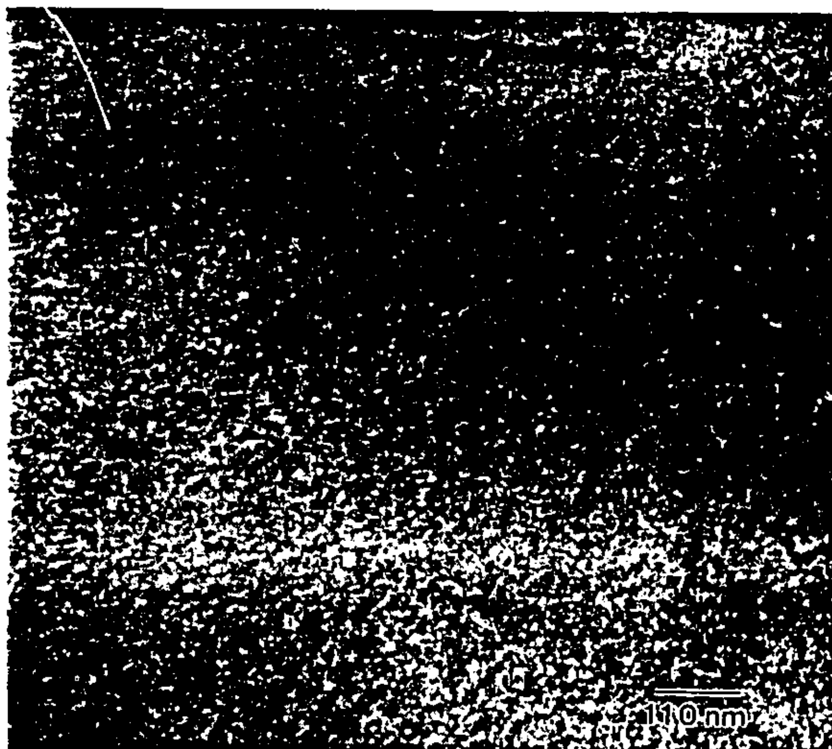

Fig. 7.2 TEM bright field micrograph of single crystal InP prepared by ion milling at liquid nitrogen temperature. Note the absence of In islands and evidence of radiation damage.

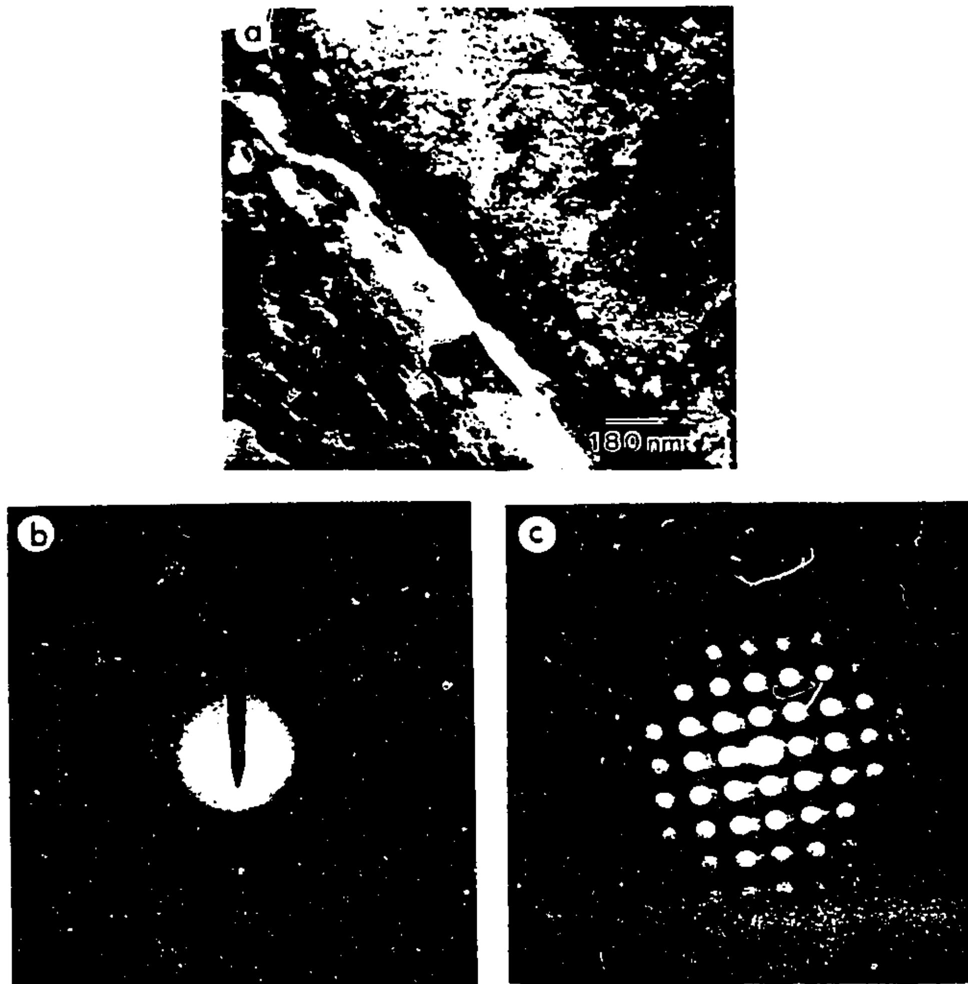

Fig. 7.3 TEM micrographs of single crystal InP prepared by photochemical etching. a) Bright field micrograph. b) Selected area electron diffraction pattern illustrating that the edge of the thin region is amorphous. c) Convergent beam electron diffraction pattern of the region adjacent to the amorphous area showing no signs of preparation induced structural artifacts.

were of very high quality and only on rare occasion were features worthy of examination found. However, samples mechanically polished with 1 μm particles showed signs of a high degree of damage. Fig. 7.4a shows a sample photochemically thinned from one side, the other side being polished with 1 μm alumina particles. The micrograph shows substantial damage in the form of finely spaced dark and light regions presumably stacking faults. The corresponding diffraction pattern in Fig. 7.4b shows spot splitting and a tendency to ring formation indicative of a highly deformed single crystal [46]. Identical features were also seen in samples prepared by one sided chemical thinning and therefore are not an artifact of the photochemical thinning process.

It has been reported that the surface of InP after a treatment with a Br-MeOH solution is phosphorous depleted [47]. To test for preferential chemical leaching, one sample from each method of preparation was randomly chosen for compositional analysis using energy dispersive analysis of X-rays (EDAX). The samples were held in a beryllium double tilt holder, and the tests were performed in one session using similar microscope conditions. The only sample to show signs of electron beam induced contamination was the one prepared by chemical thinning. However, the contamination spots were not present after each sampling and therefore contamination was not a significant problem. The EDAX results showing the raw

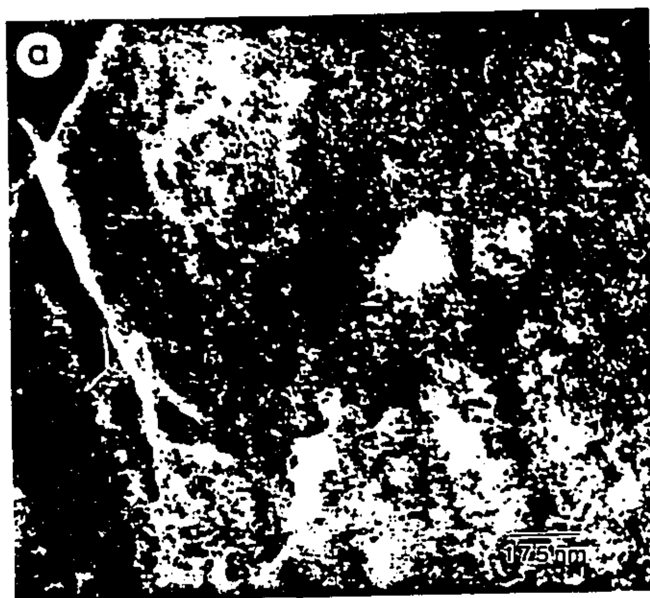

Fig. 7.4 InP single crystal photochemically thinned. a) Bright field micrograph showing structure of a surface prepared by polishing with 1 μm sized particles. b) Corresponding selected area electron diffraction pattern showing spot splitting indicative of a high degree of crystal damage.

X-ray counts for the three types of samples using identical windows are shown in Table 7.1. The results represent the average X-ray counts of at least four samplings for In and P. The data show that the variation in the percentage of counts for In and P from sample to sample is on the order of ±2%. The data are the same to within the one standard deviation of the experimental mean. The data seem to indicate that regardless of the preparation method compositional information is not significantly different and therefore is not a function of the method of preparation.

7.3 Thickness of Photochemical Oxide

The nature of surface oxides on InP is a very popular area of research because of the promise for semiconducting metal-oxide-semiconductor (MOS) technology [48]. The chemical composition and thickness of native, thermal, and anodic oxides is specific to the particular conditions of growth. Native oxide properties are a function of surface chemical pretreatment and storing environment [47,49,50]. In one instance the thickness of the native oxide was estimated by angle resolved X-ray photoelectron spectroscopy (XPS) to be 0.9 nm for n-InP [49]. Thermal and anodic oxides are also very sensitive to processing and growth conditions.

Table 7.1 Uncorrected EDAX data of InP prepared for the TEM with three different methods. The data is expressed as a percentage of total counts found in the window considering only In and P, not the elemental composition. The numbers are an average of at least four samplings.

	photoetched	Br-MeOH	ion milled
% indium	74.0±1.1	73.2±1.3	71.8±0.9
% phosphorous	26.0±1.1	26.8±1.3	28.2±0.9

Chemical homogeneity and film thickness vary with current density, acid composition, temperature and duration of growth [49,51,52]. Reported oxide thickness values vary from 6 to 60 nm, with widely varying stoichiometries.

As indicated in section 7.2, samples prepared by photochemical etching appeared to be partially covered with an amorphous film. The film is believed to be a residual oxide product of the photochemical etching process. An effort was made to determine the thickness and composition of this layer with a scanning Auger microscope (SAM) and a Tencor mechanical profilometer. If samples prepared by photochemical etching are to be examined in the TEM it is important to know the characteristics of the residual film and how the film may affect the interpretation of microstructure.

One standard method of obtaining the chemistry of surface films as a function of film depth is to perform a depth profile in the SAM. In a depth profile an elemental survey is taken followed by removal or sputtering of material using an energetic ion beam. This process is repeated until the film has been totally removed. In order to determine the film thickness it must be independently measured or the sputtering rate must be known. In very thin films (as in the case of native oxides) it is often a problem to measure film thickness accurately. A simple method of determining sputtering rates is to produce a thicker film which can be easily measured by

partially removing the layer and measuring the step height. This coupled with the time taken to remove the layer by sputtering gives the sputtering rate. Assuming that the sputtering rate for the thin and thick films are the same, the thickness of the thin film is straight forward to obtain.

The residual film thickness is very thin, on the order of a few nanometers. To try to quantify its thickness the sputtering rate for a thermally grown oxide was obtained. The oxide was grown at ≈150°C in room air for 100 hours and was 20±10 nm thick as measured with a Tencor profilometer. In the SAM, sputtering was carried out using nitrogen gas as the ion source at 1.5 kV, tilted 30° from the surface normal with an ion gun gas pressure of 10 mPa. To avoid electron beam induced changes in the surface layer, the survey area was changed from the usual spot mode to a region approximately 100 μm^2. Due to the roughness of the specimens (all samples had the 14.5 μm surface polish) the boundary between the oxide layer and the underlying bulk InP was diffuse. Consequently, the point where the surface oxide layer ended and the bulk InP began was not obvious.

The time taken to sputter through the oxide layer was arbitrarily defined as the point where the oxygen signal was below both the In and P signals and less than 20% of the total Auger signal. This definition was used in both the thermally grown oxide and the photochemically produced oxide. The time

taken to sputter through the thermal oxide was 15 minutes resulting in a sputtering rate of 1.33 nm/min. The time taken to sputter through the photochemically grown oxide was 2.5 minutes. Assuming that the sputtering rates for the two oxides are similar, the oxide thickness on the photochemically prepared sample was 3-4 nm thick.

The stoichiometry of the oxides taken from the Auger atomic concentration profile data without standards were $(In_{1+x}P_{1-x})O_4$ with x=0.25 and $\approx(InP)_2O_3$ for the thermal and photochemical oxides respectively. In a separate test the stoichiometry of the native oxide was also found to be $\approx(InP)_2O_3$. This coupled with the fact that the thickness of the photochemically grown oxide is comparable to that of the native oxide raises an interesting point. The point is that the oxide believed to be photochemically grown may actually be the native oxide formed after photoetching and the photochemical oxide is actually much thinner than the reported 3-4 nm. It is difficult to address this problem without some means of insitu monitoring in order to avoid the formation of a native oxide. However, it is conservative to conclude that the thickness of the photochemical oxide is 3-4 nm and most probably much less than that.

7.4 Application to Substrates Containing Epitaxial Layers

As outlined above InP wafers were successfully prepared for examination in the TEM. However, thinning wafers is much easier than thinning a semiconductor device containing multiple layers. In an attempt to bridge the gap between thinning wafers and thinning devices, wafers containing epitaxially grown layers of various compositions were obtained.

In order to examine a specific layer the thinning process needed to be accurately controlled. The layer of interest had a composition of $In_{0.73}Ga_{0.27}As_{0.6}P_{0.4}$ with a wavelength of 1.3 μm. Thinning down to this layer was accomplished by monitoring the PL signal from the wafer as it was being thinned from the substrate side to the epi-layer side. When light of this wavelength was detected the thinning process was terminated and the sample was ready for the microscope.

Some examples of the PL signal from three different samples are shown in Fig. 7.5a-c. Figs. 7.5a and b show that the PL signal is specimen specific and that in some instances, due to the very low PL signal, the ability to isolate the desired layer may not be possible. The low PL signal is believed to indicate that the layer is of poor quality and/or very thin. Fig. 7.5c shows one sample in which the etching process was terminated by the PL signal.

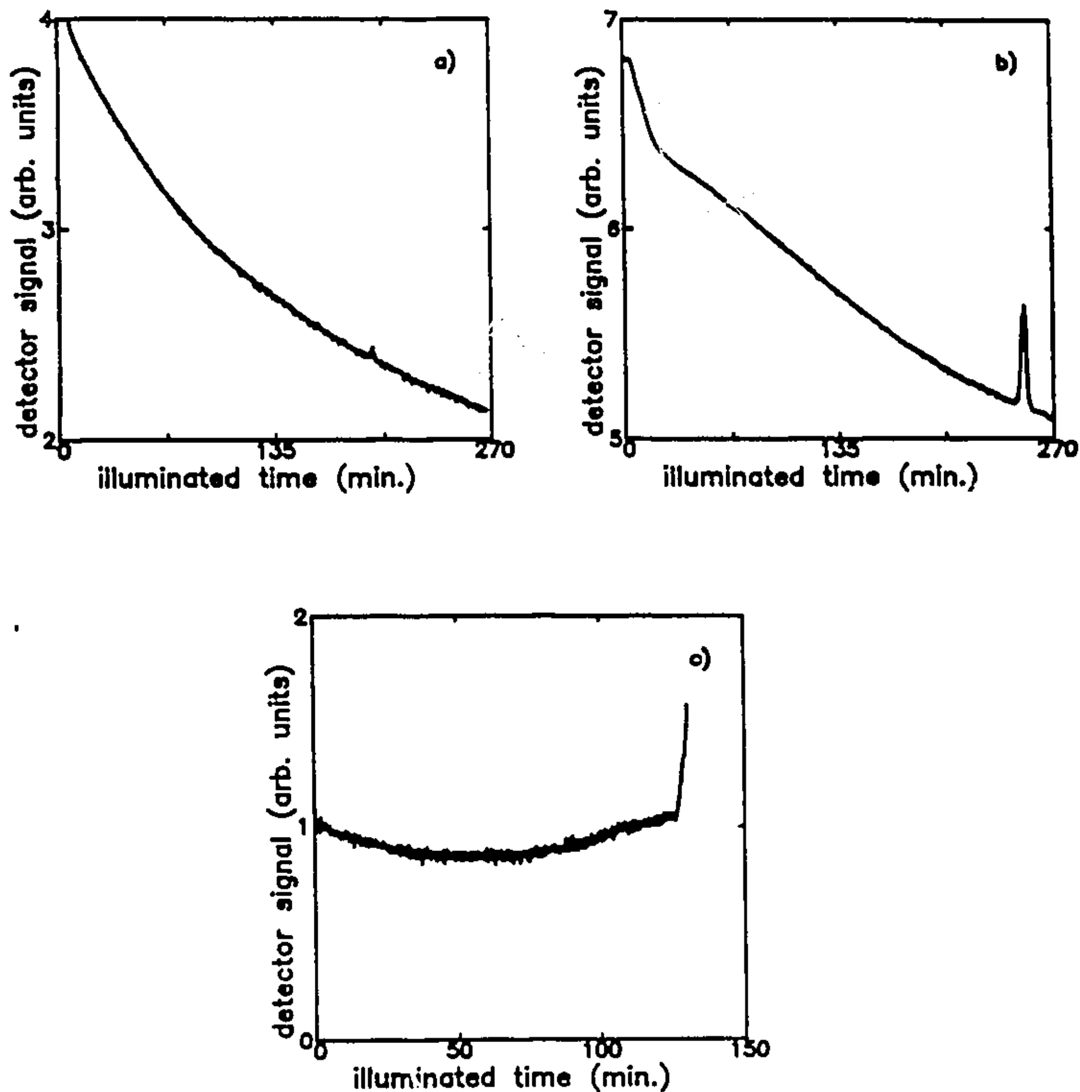

Fig. 7.5 Photoluminescence (PL) signal from wafers containing a quaternary layer while being etched. a) A sample with a low signal indicating a thin and/or poor quality layer. b) A sample with a strong signal. c) A sample with a strong signal for which the etching process was terminated in the quaternary layer using computer soft ware.

The criteria for termination is controlled through soft ware. Thus, the sensitivity or accuracy in controlling the termination point is readily achieved even to the point where epi-layer interfaces may be isolated. Samples prepared in this manner showed no signs of unusual microstructure associated with the epi-layers.

7.5 Summary

The application of photochemical etching to produce thin foils for examination in the transmission electron microscope was presented and evaluated. This new technique was compared on a qualitative and quantitative basis to two other widely used sample preparation methods.

The main limitation to this technique is the size of the thin regions. However, this limitation does not preclude its use, as the technique was developed for thinning semiconductor devices with regions of interest on the order of a few square microns. This limitation is easily overcome by using a light source that has sufficient irradiance ($\approx$200 W/cm^2) with a large illumination area, or by moving the laser beam over the sample surface to remove large volumes of material as discussed in Chapter 6. The main advantage of this technique is the ability to thin precisely predetermined regions and

that these regions are surrounded with a thick built-in stabilizing structure.

The techniques evaluated all exhibited some form of preparation artifact. However, it was shown that the artifacts produced were either avoidable or they did not significantly interfere with the ability to examine microstructure.

The feasibility of this new technique for thinning semiconductor devices was also demonstrated. By monitoring the PL signal from the layer to be isolated the thinning process was easily and accurately terminated. It should be noted that this technique applies only to n-type substrates.

Chapter 8. Summary and Recommendations for Further Research

8.1 Introduction

This chapter is divided into three subsections, section two discusses some areas which show promise for future research, and section three summarizes the major contributions of the work to the advancement of knowledge in science.

8.2 Recommendations for Further Research

The research carried out and reported in this thesis has identified many different areas in need of further research. These areas will be addressed in the order in which they arose in the thesis.

It was clear from Chapter 3 that the rate equation model for the removal of material fit the experimental data for a wide range of experimental conditions including temperature, irradiance, frequency and duty cycle. The model was based upon a fairly simple physical picture which predicted that low duty cycle light was much more efficient than continuous illumination. In order to test the model and explore the

limits of the low duty cycle etching (<5%) an acousto optic modulator (AOM) was used. The AOM diffracted the incident laser beam with duty cycles varying from 50 to 0.02% at 200 Hz. For all experiments the first order diffracted beam was used as the etching beam. The incident laser power was adjusted so that the power in the first order diffracted beam was 4 mW at a wavelength of 488 nm. The extinction ratio (the ratio of power in the first order beam when the light is diffracted to when it is not diffracted) was measured as 1 part in 300. This light level corresponds to 13 μW, and when tested at 100% duty cycle showed no visible signs of etching.

The data taken at 20°C using the AOM at 200 Hz is shown in Fig. 8.1. Data for duty cycles already reported using a mechanical chopper were repeated using the AOM to ensure that results obtained with the two chopping methods were the same and therefore interchangeable. The results showed that within experimental scatter the data were the same. Fig. 8.1 shows that the PER continued to increase with duty cycle down to 0.02%. This lowest duty cycle corresponded to a 1 μs pulse of light followed by 5 ms of dark time. Comparing samples etched with a 2.5 ms pulse (50% duty cycle) and a 1 μs pulse (0.02% duty cycle), the amount of time taken for sample perforation was an order of magnitude larger, however, the illumination time was 2500 times less for vias etched using 1 μs pulses. By interrupting the light flux, the PER increased representing

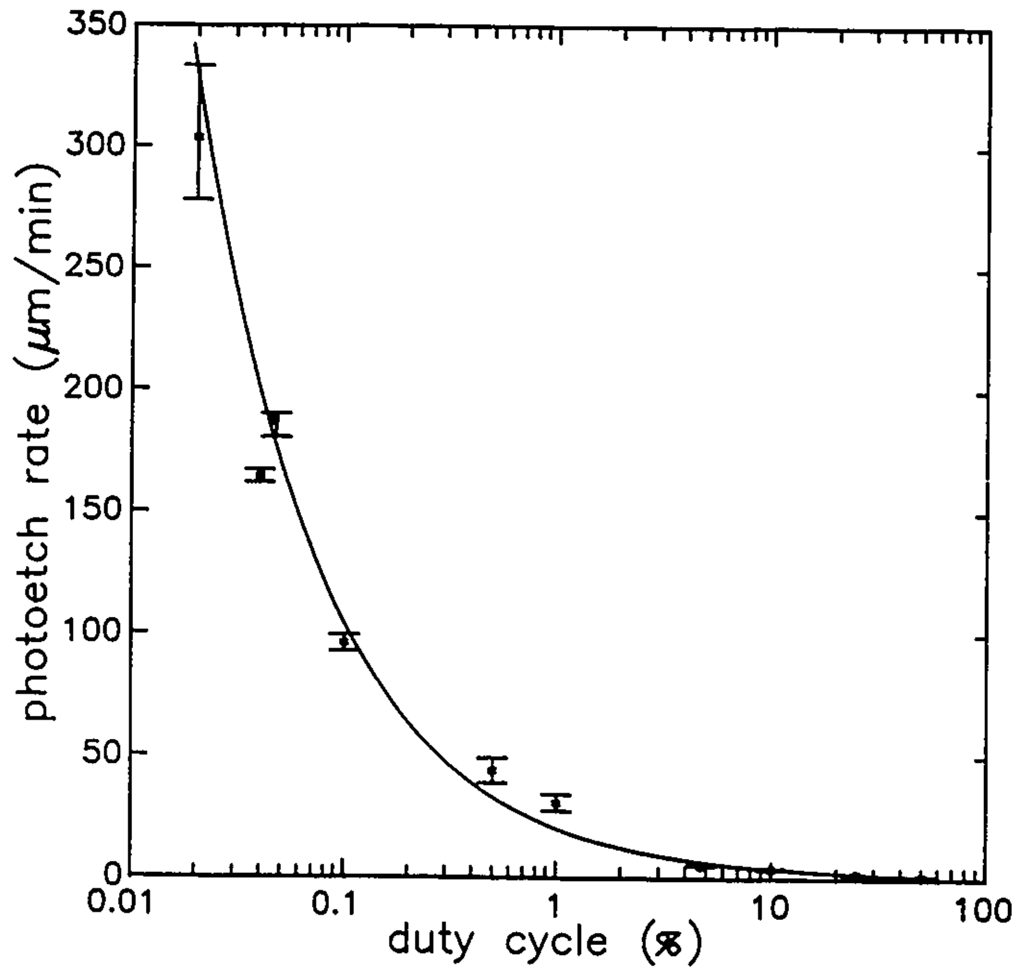

Fig. 8.1 PER versus duty cycle using the AOM at 200 Hz and 20°C. The solid line represents a best fit to the experimental data. The equation is: PER = 20*(duty cycle)$^{(-0.71)}$.

a significant improvement in photon efficiency. This indicates that pulsed light with high irradiance and low duty cycle would be an effective source for photochemical etching of n-InP. The most efficient duty cycle was not determined, however, it must lie between 0 and 0.02% as the rate of etching is essentially zero in the dark.

As seen in Chapter 3, the model successfully predicted the correct photoetching behaviour for duty cycles above 5%, however, using the fitting parameters from Figs. 3.5 and 3.7, the model is capable of predicting the correct behaviour only for duty cycles between 10 and 100%. This is shown in Fig. 8.2 where the solid curve represents the experimental data, and the lower dashed curve is that predicted by the model using the fitting parameters from Chapter 3. When the fitting parameters were changed a better fit to the experimental data was obtained as shown by the upper dashed curve in Fig. 8.2 using $I=368$, $k=145$, and $\alpha=210$. The fit to the experimental data is accurate for duty cycles >10% and then much less accurate in predicting the actual PER data for lower duty cycles. Also, it is possible to select the fitting parameters to accurately predict the PER data for low duty cycles but the fit for duty cycles greater than 5% becomes poor. Although the model is not capable of accurately predicting the PER over all duty cycles, it is successful in predicting the PER trends as a function of frequency,

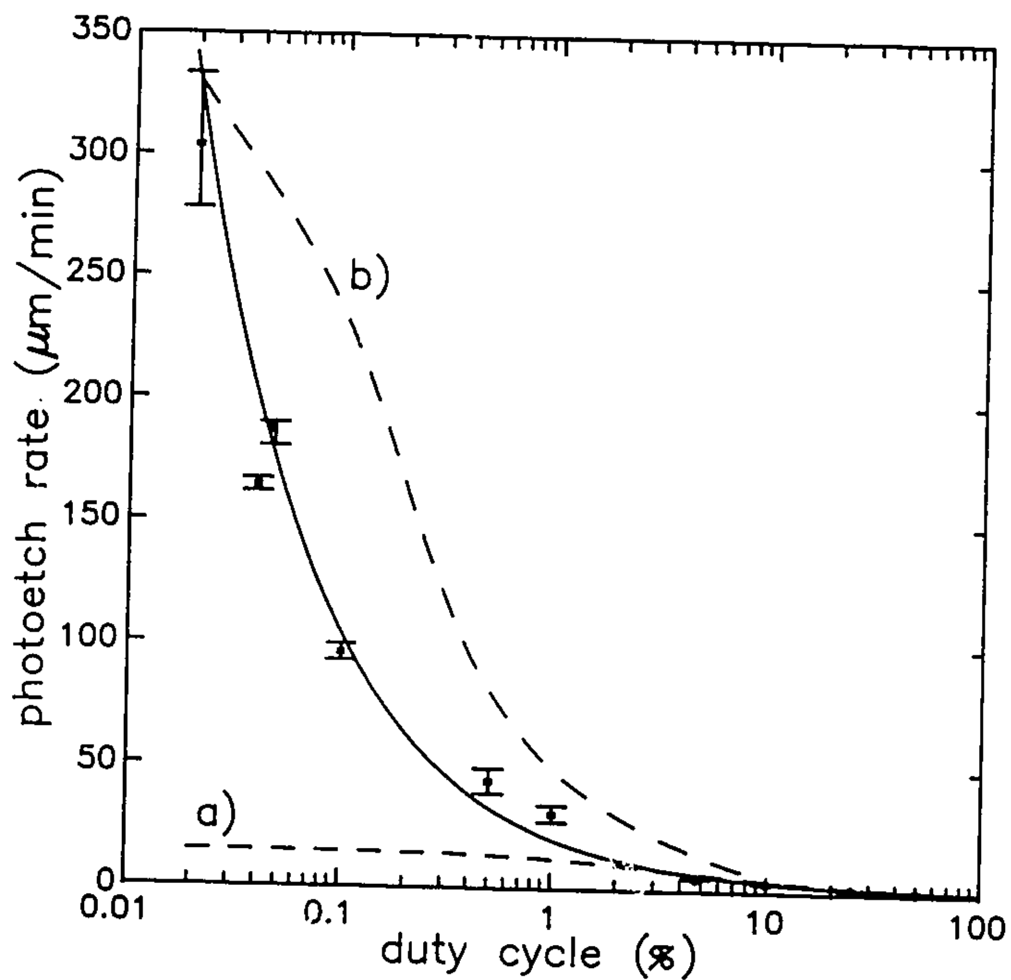

Fig. 8.2 PER data obtained with the AOM as predicted by the model of Chapter 3 with a) I=15, k=55, and α=84 and b) I=368, k=145, and α=210.

temperature, irradiance, and duty cycle including a saturation of PER as duty cycle tends to zero.

Clearly the initial model is an over simplification of the photoetching process and is in need of further study. To predict accurately the PER the initial assumptions used to develop the model must be modified. One possible modification is to allow the rate of reaction to be a function of the amount of time the light is on. As the length of time on increases the rate of reaction would decrease because the photon efficiency rapidly decreases with time. Additional photoetching data at very low duty cycles (<0.02%) at frequencies other than 200 Hz is another area that is recommended for further study. This work could lead to an enhanced understanding of the photoetching process.

From Chapter 4, the need for a comprehensive electrochemical study is apparent. A project such as this would greatly help in the understanding, both thermodynamic and kinetic, of charge transfer mechanisms at the semiconductor/electrolyte interface which would help to clarify the physical picture of the photoetching process. In the context of Chapter 4 and 5, not only would it help explain the saturation of PER at $\approx$1.2 μm/min (with copper ions in solution or gold wire bonds to the surface), it would also help in the understanding of increasing PER with surface roughness.

The work outlined in Chapter 6 provides a vast amount of material for future research. Some obvious questions pointing to new areas in need of additional research with potentially new engineering applications are: why was the work in contradiction with previous work; how many vias can be etched simultaneously before the PER becomes adversely affected; what are the possibilities for surface sculpting; and how can this data and knowledge be most effectively used for processing semiconductor surfaces.

The work presented in Chapter 7 has opened a whole new area of research possibilities. The production of semiconducting materials and devices for the TEM by photochemical etching was demonstrated, however, more effort is required to develop this technology to it fullest potential. The issue of residual oxide thickness and composition on the photoetched samples is also in need of further study.

Some additional more general areas that could be studied in the context of this work are how the PER is affected by changing the electrolyte chemistry, biasing the sample during etching, and using different wavelengths as the illumination source.

8.3 Summary

This project was undertaken to examine the microstructure of semiconductor diode lasers in an effort to try to relate material changes to device degradation. The TEM was selected as the tool for examining microstructure. Due to the small size of the diode lasers, difficulties with specimen preparation and handling for the TEM had to be addressed. The proposal was to thin the specimens using a technique known as photochemical etching. In order to employ effectively this technique the photoetching process was thoroughly investigated.

The photoetching process was found to be reaction rate limited with a thermal activation energy of $\geq 0.34\pm 0.03$ eV. The photoetching behaviour was studied as a function of irradiance, duty cycle, and frequency of the incident illumination. The process was modelled based on the rate of generation and removal of reaction products under the illuminating source. The model was capable of predicting the experimentally observed trends for various temperatures, frequencies, irradiance levels, and duty cycles down to 0.02%. It was possible to increase the PER by over an order of magnitude to ≈ 13 μm/min by increasing the etchant temperature, and over two orders of magnitude to ≈ 300 μm/min by varying the duty cycle at room temperature.

The PER was also found to be dependent upon the impurities present in the electrolyte. With certain metal ions in solution, and with gold wire bonds to the sample surface, the PER was significantly enhanced. A mechanism involving an alternate pathway for electron transfer at the semiconductor/electrolyte interface accounting for the enhancement of PER was proposed and evidence supporting the proposal was presented.

The effect of surface quality and preparation on the PER was also extensively studied. The PER was found to be dependent upon the effective surface area available for the photochemical reactions taking place on the sample when no copper ions were in solution or no gold wire bonds were attached to the sample surface. The effective surface area of the sample could be controlled by altering the physical dimensions of the sample or by changing the size and/or morphology of the polishing media.

The PER was found to saturate at ≈ 1.2 $\mu m/min$ for samples with metal ion impurities in the electrolyte and gold wire bonds to the surface for irradiance levels up to ≈ 800 W/cm^2 and effective surface areas of $\approx 10^7$ μm^2. Saturation of the PER was locally controlled. This was determined by etching vias with one and two light sources simultaneously and noting that no significant difference in the PER occurred for the two different situations. Local saturation of the PER has

significant implications for applications in semiconductor surface sculpting and processing.

The initial goal of the research project was to prepare semiconductor samples for microstructural evaluation in the TEM by photochemical etching. This goal was realized as it was demonstrated that this technique was capable of producing semiconductor samples with complex structures for examination in the TEM. Two advantages over traditional preparation methods are that there is a built in stabilizing structure which helps protect thinned regions from fracture and the ability to thin precisely predetermined regions for microstructural evaluation. In addition to realizing the initial goal, original contributions to the subject of photochemical etching were made.

References

1. G.P. Agrawal, and N.K. Dutta, Long-wavelength Semiconductor Lasers, Van Nostrand Reinhold Co., Inc., New York, 1986.

2. Yu.L. Khait, J. Salzman, and R. Besserman, Appl. Phys. Lett., 53, 2135 (1988).

3. S.N.G. Chu, S. Nakahara, M.E. Twigg, L.A. Koszi, E.J. Flynn, A.K. Chin, B.P. Segner, and W.D. Johnston, Jr., J. Appl. Phys., 63, 611 (1988).

4. S.N.G. Chu, S. Nakahara, L.C. Luther, and H.W. Krautter, J. Appl. Phys., 69, 6974 (1991).

5. R.M. Lum, F.W. Ostermayer, Jr., P.A. Kohl, A.M. Glass, and A.A. Ballman, Appl. Phys. Lett., 57, 269 (1985).

6. J.E. Bjorkholm, and A.A. Ballman, Appl. Phys. Lett., 43, 574 (1983).

7. G.C. Chi, F.W. Ostermayer, Jr., K.D. Cummings, and L.R. Harriott, J. Appl. Phys., 60, 4012 (1986).

8. A.E. Willner, M.N. Ruberto, D.J. Blumenthal, D.V. Podlesnik, and R.M. Osgood, Jr., Appl. Phys. Lett., 54, 1839 (1989).

9. D.V. Podlesnik, H.H. Gilgen, and R.M. Osgood, Jr., Appl. Phys. Lett., 45, 563 (1984).

10. C. Frigeri, and J.L. Weyher, J. Appl. Phys., 65, 4646 (1989).

11. J.L. Weyher, and J. van de Ven, J. Crystal Growth, 78, 191 (1986).

12. Yu.V. Pleskov, and Yu.Ya. Gurevich, Semiconductor Photoelectrochemistry, Consultants Bureau, New York, 1986.

13. A.B. Ellis, J.M. Bolts, and M.S. Wrighton, J. Electrochem. Soc., 124, 1603 (1977).

14. K. Ozawa, T. Ito, and H. Ishikawa, Jpn. J. Appl. Phys., 26, 1509 (1987).

15. L.A. DeLouise, J. Appl. Phys., 70, 1718 (1991).

16. J. ven de Van, and H.J.P. Nabben, J. Electrochem. Soc., 137, 1603 (1990).

17. J. van de Ven, and H.J.P. Nabben, J. Electrochem. Soc., 138, 144 (1991).

18. A.E. Willner, D.V. Podlesnik, H.H Gilgen, and R.M. Osgood, Jr., Appl. Phys. Lett., 53, 1198 (1988).

19. T.D. Lowes, and D.T. Cassidy, J. Appl. Phys, 68, 814 (1990).

20. T.D. Lowes, and D.T. Cassidy, Second International Conference on InP and Related Materials, Conference Proceedings, p203, April 23-25, 1990, Denver, Colorado, IEEE Catalog #90CH2859-7.

21. T.D. Lowes, and D.T. Cassidy, submitted to J. Electrochem. Soc., August 1991.

22. T.D. Lowes, and D.T. Cassidy, submitted to Semiconductor Science and Technology, May 1992.

23. T.D. Lowes, and D.T. Cassidy, submitted to J. Electron Microscopy Technique, November, 1991.

24. M.N. Ruberto, X. Zhang, R. Scarmozzino, A.E. Willner, D.V. Podlesnik, and R.M. Osgood, Jr., J. Electrochem. Soc., 138, 1174 (1991).

25. M. Lax, J. Appl. Phys., 48, 3919 (1977).

26. M.N. Ruberto, A.E. Willner, D.V. Podlesnik, and R.M. Osgood, Jr., Appl. Phys. Lett., 55, 984 (1989).

27. D.V. Podlesnik, H.H. Gilgen, and R.M. Osgood, Jr., Appl. Phys. Lett., 48, 496 (1986).

28. M. Otsubo, T. Oda, H. Kumable, and H. Miki, J. Electrochem. Soc., 123, 676 (1976).

29. J. Chen, S. Lee, and T. Ho, J. Electrochem. Soc., 132, 3016 (1985).

30. J. van de Ven, J.E.A.M. van der Meerakker, and J.J. Kelly, J. Electrochem. Soc., 132, 3020 (1985).

31. S. Iida, and K. Ito, J. Electrochem. Soc., 118, 768 (1971).

32. K.D. Cummings, L.R. Harriott, G.C. Chi, and F.W. Ostermayer, Jr., Appl. Phys. Lett., 48, 659 (1986).

33. M. Pourbaix, Atlas of Electrochemical Equilibria in Aqueous Solutions, Pergammon Press, Toronto, 1966.

34. T. Kawai, K. Tanimura and T. Sakata, Chem. Lett., 137 (1979).

35. H. Gerischer, B. Pettinger, and M. Lubke, Symposium on Electrocatalysis, Electrochem. Soc., San Francisco, p160 (1974).

36. G.C. Bond, Catalysis by Metals, Academic Press Inc., New York, 1964.

37. J.J. Kelly, J.E.A.M. van den Meerakker, P.H.L. Notten, and R.P. Tijburg, Philips Technical Review, 44, 61 (1988).

38. CRC Handbook of Chemistry and Physics 60th Edition, R.C. Weast ed., CRC Press, Inc., Boca Raton, Florida, 1980.

39. R.D. Coombe, and F.J. Wodarczyk, Appl. Phys. Lett., 37, 846 (1980).

40. W. Ahmed, private communication, Buehler Limited, Evanston, Illinois.

41. K.D. Cummings, L.R. Harriott, G.C. Chi, and F.W. Ostermayer, Jr., Appl. Phys. Lett. 48, 659 (1986).

42. O.J. Glembocki, and H. Piller, Handbook of Optical Constants of Solids, E.D. Palik ed., Academic Press, Inc., Toronto, p508, 1985.

43. P.T. Landsberg, The Inst. of Elec. Eng. 106B, 908 (1959).

44. N.G. Chew, and A.G. Cullis, Ultramicroscopy, 23, 175 (1987).

45. O. Wada, J. Phys. D: Appl. Phys., 17, 2429 (1984).

46. P. Hirsch, A. Howie, R. Nicholson, D.W. Pashley, and M.J. Whelan, Electron Microscopy of Thin Crystals, Robert E. Krieger Publishing Co., Inc., Malabar, Florida, 1977.

47. L. Henry, A. Le Corre, D. Lecrosnier, M. Gauneau, C. Vaudry, P. Alnot, J. Olivier, and S.K. Krawczyk, Second International Conference on InP and Related Materials, Conference Proceedings, p234, April 23-25, 1990, Denver, Colorado, IEEE Catalog #90CH2859-7.

48. L.G. Meiners, and H.H. Wieder, Materials Science Reports, 3, 143 (1988).

49. A. Hofmann, P. Steubel, and A. Meisel, Surf. and Int. Anal., 12, 315 (1988).

50. O. Oda, K. Katagari, K. Shinohara, S. Katsura, Y. Takahashi, K. Kainosho, K. Kohiro, and R. Hirano, in Semiconductors and Semimetals, Vol. 31, InP: Crystal Growth and Characterisation, R.K. Willardson, and A.C. Beer eds., Academic Press, Inc., Toronto, p94, 1990.

51. K. Durose, M.R. Aylatt, and J. Haigh, Chemtronics, 3, 201 (1988).

52. G. Hollinger, J. Joseph, Y. Robach, E. Bergignat, B. Commere, P. Viktorovitch, and M. Froment, J. Vac. Sci. Technol., B5, 1108 (1987).